ICARUS 67, 134–163 (1986)

Structure of the Uranian Rings

II. Ring Orbits and Widths

R. G. FRENCH,* J. L. ELLIOT,*,† AND S. E. LEVINE*

*Department of Earth, Atmospheric, and Planetary Sciences, and †Department of Physics, Massachusetts Institute of Technology, Cambridge, Massachusetts 02139

Received October 17, 1985; revised March 17, 1986

We have used the square-well model of J. L. Elliot, R. G. French, K. J. Meech, and J. H. Elias (1984, *Astron. J.* **89,** 1587–1603) to determine the midtimes, widths, and optical depths of all available Uranus ring occultation observations from 1977 to 1983. We have fitted an improved kinematical model for the nine known rings, from which we find: (i) $J_2 = (3.3461 \pm 0.0030) \times 10^{-3}$, $J_4 = (-3.21 \pm 0.37) \times 10^{-5}$, pole of the equatorial plane (1950.0) $\alpha = 5^h06^m25.6^s \pm 4.6^s$, $\delta = +15°01'56'' \pm 2'09''$; typical uncertainties in ring orbital elements are as follows: σ(semimajor axis) $\simeq 5$ km, σ(eccentricity) $\simeq 2 \times 10^{-5}$, σ(inclination) $\simeq 0.005°$; (ii) typical post-fit residuals of 0.2–0.6 km in the ring plane radius for rings 6, 5, 4, α, β, η, and ε are comparable to the uncertainties in the midtimes for many data sets; (iii) upper limits to shepherd satellite masses of $m < 10^{18}$ g $(\Delta/100\text{ km})^2$ for shepherds near these seven rings, from observed radial perturbations, and $m < 4 \times 10^{17}$ g $(\Delta/100$ km)^2 from anomalous ring precession rates (where Δ is the distance between the ring and the shepherd satellite); (iv) the γ and δ rings have rms radial perturbations $\simeq 3$ km, well above the uncertainties in the occultation profile midtimes; (v) these perturbations appear to vary slowly with true anomaly, raising the possibility that they may be associated with Lindblad resonances.

From the ring width determinations, we find: (vi) all nine rings have significant width perturbations, well above the uncertainties in the width measurements; (vii) typical width perturbations are 0.5–2.0 km, much larger than the orbit radius perturbations for all but the γ and δ rings; (viii) newly determined width–longitude relations, including apsidal twists, and dynamical models yield ring masses of $(4.2 \pm 0.9) \times 10^{16}$, $(3.8 \pm 0.6) \times 10^{16}$, and $(6.1 \pm 0.1) \times 10^{18}$ g, surface densities of 2.0 ± 0.4, 1.5 ± 0.2, and 32.9 ± 0.6 g cm^{-2}, and dispersion velocities of 0.15 ± 0.03, 0.17 ± 0.02, and (0.17 ± 0.25) cm sec^{-1} for the α, β, and ε rings, respectively, and a typical ring thickness of $\simeq 8$ m, consistent with the results of P. D. Nicholson and K. Matthews (1983, *Bull. Amer. Astron. Soc.* **15,** 816); (ix) there are significant deviations (>1 km) from the best-fitting sinusoidal width–longitude relations for the α, β, and ε rings; (x) the narrow eccentric rings 6, 5, and 4 do not follow simple width–longitude relations; (xi) the quasi-circular rings η, γ, and δ show large width variations (greater than a factor of 2), even for ring profiles at the same true anomaly obtained at different times.

From optical depth measurements of the rings, we find: (xii) accurate width–optical depth products ("equivalent depths"), based on a square-well model, for profiles of all nine rings; (xiii) the rings are not optical monolayers—there is significant particle shadowing for all nine rings; (xiv) the "equivalent depths" of the γ and δ rings are not conserved, probably indicative of unresolved radial structure within the rings.

I. INTRODUCTION

Since the discovery of the Uranian rings in 1977, several hundred ring occultation profiles have been obtained by many observers. These observations provide the basis for our current understanding of the radial structure and orbital kinematics of the rings, but heretofore they have not been analyzed in a self-consistent fashion to obtain widths, optical depths, and midtimes, along with errors in these quantities. This is necessary if we are to improve our knowledge of the details of the structure of the Uranian rings. For example, width–longitude relations have been established for the α, β, and ε rings, but not for any others (Elliot and Nicholson, 1984). Wavy edges, tell-

0019-1035/86 $3.00

tales of shepherd satellites, have been found in some of Saturn's rings (Cuzzi and Scargle, 1985)—are there similar clues in the Uranian rings? As a final example, the investigation of orbit perturbations, by shepherd satellites or other causes, requires precise determination of the ring orbital elements, possible only if the midtimes of the occultation profiles are accurately known.

In Paper I of this series (Elliot *et al.*, 1984), we described a square-well model for occultation profiles produced by the Uranian rings, which we used to determine the relative optical depths of the rings at visible and near-infrared wavelengths. In this paper, we present comprehensive results of our analysis of all available occultation observations obtained from 1977 to 1983. First, in Section II, we survey the available data and use the square-well model to determine ring widths, optical depths, and midtimes. In Section III, using the midtimes so obtained, we refine our solution for the orbits of the rings. We use these results to place limits on the masses of possible shepherd satellites, and to investigate other possible causes of orbit perturbations. In Section IV, we examine the variation of ring width with orbital longitude, both to improve the width–longitude relations of the α, β, and ε rings and to determine whether or not the other rings have simple width–longitude relations as well. In Section V, we investigate the structure of the rings to determine their mean opacities and whether they are monolayers or are many particles thick. Finally, in the last section, we discuss our results and present our conclusions.

II. SURVEY OF OCCULTATION OBSERVATIONS

In order to obtain accurate widths and midtimes (and their errors) from ring occultation profiles, it is desirable that the data be digitally recorded at high time resolution, that the relative contributions of the star, rings, planet, and sky be well determined, and that accurate absolute timing be maintained. In fact, these conditions have rarely been fully satisfied. The hundreds of available ring profiles have been obtained from more than a dozen occultations, by observers at many different sites, using a variety of equipment. There is, inevitably, considerable variation in the quality of the data. It is useful, therefore, to survey the complete set of available observations to assess their utility for detailed analysis.

Table I (after Elliot and Nicholson, 1984) summarizes all known successful observations of the Uranian rings through the 1984 aparition, and indicates their utility for occultation timing and for ring width determination. Only data recorded on magnetic tape are useful for ring timing, since strip chart records are difficult to calibrate accurately in absolute time, often move at uneven rates, and suffer from digitization errors when transcribed for computer analysis. Generally speaking, ring widths are obtainable from strip chart profiles, but are accurate only for the widest of the rings.

The adopted stellar diameters for each occultation are given in Table II. These were computed using V–K photometry and the results of K. J. Meech (private communication, 1985), assuming a limb-darkening parameter $b = 1$ [see Paper I, Eq. (8)].

Each occultation is discussed in more detail below, and the results of model fits to the ring profiles are tabulated. Except as noted, the free parameters in the fits were (see Table I, Paper I) $\bar{n}_f$, the full scale counting rate, t_o, the ring midtime, T_o, the duration of the event, A_o, the equivalent depth, and $\dot{n}_b$, the background slope, in those few cases where it was large. All other model parameters were held fixed. Widths and equivalent depths are omitted from the tables if their estimated uncertainty is greater than two-thirds the fitted values.

10 March 1977. The discovery occultation was observed from six sites, as summarized in Table I. Elliot *et al.* (1978) used

TABLE I

Observations of Occultations by the Uranian Rings

Date	Star	Station	Primary Recording Medium	Used in present analysis : Midtimes	Used in present analysis : Widths	References
10 Mar. 1977	SAO 158687	KAO	magnetic tape	Y	Y	Elliot *et al.* (1984)
		Perth (Lowell)	strip chart	N	N	Millis *et al.* (1977a,b)
		Perth (Arizona)	magnetic tape	N	N	Hubbard and Zellner (1980)
		Kavalur	strip chart	N	N	Bhattacharyya and Bappu (1977)
		Naini Tal	strip chart	N	N	Mahra and Gupta (1977)
		Peking	strip chart	N	N	Chen *et al.* (1978)
		Cape	strip chart	N	N	Elliot *et al.* (1978)
23 Dec. 1977	KM2	Tenerife	magnetic tape	N	N	Millis and Wasserman (1978)
4 Apr. 1978	KM4	LCO	strip chart	N	N	Nicholson *et al.* (1978)
10 Apr. 1978	KM5	LCO	strip chart	N	Y	Nicholson *et al.* (1978)
10 June 1979	KM9	LCO	strip chart	N	Y	Nicholson *et al.* (1981)
20 Mar. 1980	KM11	CTIO	magnetic tape	Y	Y	Elliot *et al.* (1978)
		SAAO	strip chart	N	Y	This work
15 Aug. 1980	KM12	CTIO	magnetic tape	Y	Y	Elliot *et al.* (1981a)
		ESO	magnetic tape	Y	Y	Sicardy *et al.* (1982b)
		LCO	strip chart	N	Y	Nicholson *et al.* (1982)
26 Apr. 1981	KME13	AAT	magnetic tape	N	Y	French *et al.* (1982)
		Kavalur	strip chart	N	Y	Mahra *et al.* (1983)
22 Apr. 1982	KME14	CTIO	magnetic tape	Y	Y	Elliot *et al.* (1984)
		ESO	magnetic tape	Y	Y	Sicardy *et al.* (1982a)
		LCO	magnetic tape	Y	Y	Unpublished
		Tenerife	magnetic tape	Y	Y	Millis *et al.* (1986)
		OPMT	magnetic tape	N	N	Sicardy *et al.* (1982a)
		Brazil	magnetic tape	Y	Y	Jablonski and Barroso (1985)
1 May 1982	KME15	Mt. Stromlo	magnetic tape	Y	N	French *et al.* (1986a)
4 June 1982	KME16	Palomar	magnetic tape	N	N	Unpublished
3 Mar. 1983	KME17a	Perth	strip chart	Y	Y	IAUC 3784 (1983)
25 Mar. 1983	KME17b	SAAO	magnetic tape			Unpublished

these observations to determine orbital characteristics of the rings. Of the six data sets, only the Kuiper Airborne Observatory (KAO) and Arizona group Perth observations were recorded on magnetic tape, and timing was uncertain for the emersion observations by the Arizona group at Perth (Hubbard and Zellner, 1980). We have used only the KAO observations to determine ring widths and event times for this occultation.

Paper I contains a detailed description of the KAO observations and the square-well model profile which was fitted to each profile. We have extended our analysis of these data in several important respects. First, we have taken into account the instantaneous aircraft velocity when computing the apparent velocity of the star perpendicular to the ring as projected on the sky. This component of the event velocity was ignored in the analysis for Paper I. Secondly, whereas Table VI of Paper I gives formal errors only, we have computed the error bars for ring width and equivalent depth (defined in Paper I as the product of the true ring width and normal optical depth) by taking into account not only the formal errors of the fit, but also the uncertainties in the angular diameter and signal level of the occulted star, as discussed in the Appendix. Finally, we have used the new ring orbit model presented in Section III to determine the true anomaly for each ring profile. These results are given in Table III. In this and succeeding tables, immersion and emersion are designated by I and E, respectively.

TABLE II

Adopted Stellar Diameters

Occultation Date	Occulted Star	Angular Diameter (milliarcsec)	Projected Diameter at Uranus (km)
10 Mar. 1977	SAO 158687	0.55 ± 0.06	7.15 ± 0.73
10 Apr. 1978	KM5	0.055 ± 0.008	0.71 ± 0.11
20 Mar. 1980	KM11	0.057 ± 0.007	0.75 ± 0.11
15 Aug. 1980	KM12	0.11 ± 0.02	1.50 ± 0.23
26 Apr. 1981	KME13	0.19 ± 0.02	2.46 ± 0.32
22 Apr. 1982	KME14	0.54 ± 0.04	7.06 ± 0.55
1 May 1982	KME15	0.20 ± 0.03	2.60 ± 0.39
25 Mar. 1983	KME17b	0.096 ± 0.005	1.29 ± 0.07

23 December 1977. The occultation of KM2 [the second star in the list of Klemola and Marsden (1977)] was observed from a single station, at Tenerife on the Canary Islands (Millis and Wasserman, 1978). Only the ε, δ, and γ immersion events were ob

TABLE III

Results of Ring Profile Fits 10 March 1977
KAO Observations

Ring	Event	Midtime (UTC)	K.A.O. Position Lat. (deg)	K.A.O. Position Long. (deg)	K.A.O. Position Alt. (km)	Width (km)	Equiv. Width E (km)	Equivalent Depth A (km)	Frac. Trans. f_0	Normal Optical Depth	True Anomaly (deg)
6	I	20:24:48.288 ± 0.016	-50.7839	-83.7269	12.57	1.07 ± 0.58	[0.70]	1.27 ± 0.83	[0.26]	[1.19]	158.8
6	E	21:41:48.381 ± 0.019	-50.7785	-99.6037	12.57	2.39 ± 1.08	[0.68]	0.83 ± 0.40	[0.66]	[0.35]	266.3
5	I	20:24:13.213 ± 0.019	-50.7547	-83.6104	12.56	5.56 ± 0.69	[1.46]	1.73 ± 0.27	[0.70]	[0.31]	230.8
5	E	21:42:18.652 ± 0.017	-50.7543	-99.6996	12.56	4.89 ± 0.76	[1.28]	1.54 ± 0.29	[0.69]	[0.31]	339.0
4	I	20:23:51.770 ± 0.014	-50.7354	-83.5425	12.56	2.37 ± 0.94	[0.96]	1.29 ± 0.57	[0.54]	[0.54]	274.2
4	E	21:42:47.014 ± 0.033	-50.7287	-99.7937	12.56	5.52 ± 1.04	[0.95]	1.07 ± 0.22	[0.79]	[0.19]	23.0
α	I	20:20:53.833 ± 0.008	-50.5839	-82.9748	12.57	9.41 ± 0.21	[4.77]	7.11 ± 0.46	[0.42]	[0.76]	65.9
α	E	21:45:51.704 ± 0.009	-50.5670	-100.4013	12.56	7.72 ± 0.24	[3.61]	5.32 ± 0.41	[0.44]	[0.69]	178.7
β	I	20:19:33.690 ± 0.011	-50.5058	-82.7172	12.56	11.06 ± 0.28	[3.76]	4.75 ± 0.36	[0.61]	[0.43]	173.3
β	E	21:47:06.072 ± 0.007	-50.5015	-100.6374	12.57	5.77 ± 0.46	[2.97]	4.64 ± 0.55	[0.38]	[0.80]	287.7
η	I	20:17:32.931 ± 0.023	-50.3917	-82.3598	12.57	3.49 ± 1.05	[0.73]	0.84 ± 0.29	[0.76]	[0.24]	253.8
η	E	21:49:08.670 ± 0.036	-50.3826	-101.0339	12.56	2.06 ± 1.00	[0.47]	0.55 ± 0.29	[0.72]	[0.27]	10.5
γ	I	20:16:57.231 ± 0.005	-50.3570	-82.2525	12.56	3.14 ± 0.94	[2.30]	5.03 ± 1.78	[0.16]	[1.60]	318.1
γ	E	21:49:44.305 ± 0.005	-50.3457	-101.1520	12.57	3.30 ± 0.92	[2.40]	5.78 ± 2.10	[0.12]	[1.75]	75.5
δ	I	20:16:02.822 ± 0.012	-50.3028	-82.0890	12.57	7.90 ± 0.35	[3.45]	4.79 ± 0.38	[0.50]	[0.61]	353.2
δ	E	21:50:38.277 ± 0.004	-50.2895	-101.3254	12.56	2.93 ± 0.96					111.6
ε	I	20:11:46.540 ± 0.006	-50.0302	-81.3580	12.56	93.88 ± 0.48	[54.30]	89.63 ± 3.11	[0.33]	[0.95]	179.1
ε	E	21:54:05.859 ± 0.004	-50.0613	-102.0011	12.56	37.74 ± 0.38	[28.75]	80.63 ± 6.86	[0.07]	[2.14]	301.3

Notes:
1) I and E stand for immersion and emersion, respectively.
2) Numbers in square brackets were derived from other parameters in the fit.
3) Geographic coordinates derived from a linear interpolation of the inertial navigation flight log.
Errors in these quantities are uncertain, but should be no more than ± 0.01 degrees.
4) The equivalent depth of the δ ring emersion profile could not be reliably determined.

served, with a relative timing accuracy of about ±0.1 sec. These three data points are not sufficient to determine accurately the corrections to the relative positions of the planet and the star. As a result, the event geometry is not well known, and in particular, the velocity of the star perpendicular to the rings is uncertain. For this reason, we have not used these data to determine ring widths or to refine the ring orbits.

4 April 1978. The occultation of KM4 was observed only from Cerro Las Campanas Observatory (LCO), and provided no ring profiles useful for midtime or width determination (Nicholson *et al.*, 1978).

10 April 1978. The occultation of KM5 was observed from LCO (Nicholson *et al.*, 1978). Because the data were recorded only on strip charts, midtimes are not accurately known, and were not used in the new ring orbit solution described in the next section. Results of profile fits to the widest two rings (β and ε) are given in Table IV. The uneven rate of the strip chart, the difficulty of accurately and repeatably digitizing the narrow ring profiles, and the uncertainty of the overall system time constant made the results for the narrower rings unreliable. (These effects are less severe for the β and ε rings.) The error bars in Table IV take into account the measured uneven chart speed (see Appendix).

10 June 1979. The occultation of KM9 was successfully observed from LCO (Nicholson *et al.*, 1981). Because the data were recorded on strip charts, midtimes are

TABLE IV

Results of Ring Profile Fits to 10 April 1978
Observations from LCO

Ring	Event	Width (km)	Equivalent Width E (km)	Equivalent Depth A (km)	Frac. Trans. f_0	Normal Optical Depth	True Anomaly (deg)
β	I	12.78 ± 1.25	[4.08]	4.98 ± 0.69	[0.66]	[0.39]	100.5
β	E	12.40 ± 1.26	[3.68]	4.49 ± 0.59	[0.66]	[0.36]	194.5
ε	I	18.35 ± 1.31	[15.84]	46.51 ± 13.62	[0.06]	[2.53]	9.2
ε	E	75.34 ± 1.32	[45.91]	79.64 ± 8.34	[0.29]	[1.06]	114.0

Notes:
1) I and E stand for immersion and emersion, respectively.
2) Numbers in square brackets were derived from other parameters in the fit.

TABLE V

Adopted Ring Widths for 10 June 1979 Observations from LCO [Nicholson *et al.* (1981)]

Ring	Event	Width (km)	True Anomaly (deg)
ε	I	75.0 ± 1.0	118.1
ε	E	51.0 ± 1.0	282.5

Note: I and E stand for immersion and emersion.

not reliable. Furthermore, as Nicholson *et al.* (1981) point out, the low signal-to-noise ratio of the data makes it difficult to estimate the radial widths of the narrow rings, and we adopt their estimates of the ε ring width as given in Table V.

20 March 1980. Observations of the occultation of KM11 were successfully made from Cerro Tololo Interamerican Observatory (CTIO) and the South African Astronomical Observatory (SAAO). The CTIO observations have been described by Elliot *et al.* (1981b). The SAAO observations were made with an InSb photometer at 2.2 μm and were recorded on a strip chart (I. Glass, private communication, 1980). Because the full stellar intensity level was not well known, these observations are useful for determining ring widths, but not for equivalent depths. Results of profile fits to both data sets are given in Table VI.

15 August 1980. The occultation of KM12 was well observed from three nearby sites in South American (see Table I), making it possible to confirm ring features large enough to produce an occultation at all three telescopes (Elliot *et al.*, 1983). Results of profile fits are given in Table VII. For our present analysis, the CTIO and European Southern Observatory (ESO) observations were first deconvolved to remove the effects of the detector time constant, with the method described in Paper I. The LCO data were digitized from strip chart records; the error bars in Table VII take into account the uneven chart speed. There appears to be a systematic offset between the CTIO and ESO equivalent depths, indicating a probable error in the determination of the star count rate, n_*, in one or both of the data sets.

26 April 1981. The occultation of KME13 (Klemola *et al.*, 1981) was successfully observed from the Anglo-Australian Telescope (AAT) and from Kavalur. The AAT observations have been described briefly by French *et al.* (1982). The star counting rate, n_*, was well determined from calibration observations, and the baselines were quite stable throughout the occultation. At Kavalur, only the ε emersion event was observed, and n_* was not well determined. The results of profile fits are given in Table VIII. The error estimates account for the uncertainty in the angular diameter of the occulted star (Table II), using the method described in the Appendix.

22 April 1982. The occultation of KME14 was by far the most widely observed of all. Five stations obtained high-quality data, and multiple-wavelength observations made it possible to set limits on the particle size distributions of ring material (Paper I). The results of profile fits to the data are given in Table IX. The CTIO results differ from those of Paper I in two respects: the errors now include the effects of uncertainty in the size of the occulted star, and the true anomaly for each ring is based on the ring orbit model described in Section III. Observations from ESO were made using the 3.6- and 1-m telescopes. Only the 1-m results are included here, because the time constant of the detector on the larger telescope was mistakenly set at 3 sec, producing smeared profiles (B. Sicardy, private communication, 1982). The immersion ESO data were quite noisy, and have not been included in this analysis. No deconvolution was performed, because the instrumental time constant was not well known. The LCO observations were made at both visible and infrared wavelengths. Details will be published elsewhere. The results in Table IX refer to the infrared data only, which were of higher quality than the visible data. The results of model profile fits to the Tenerife observations are presented by Millis *et al.* (1986). At the Observatoire du Pic du Midi et de Toulouse (OPMT), obser-

TABLE VI

Results of Ring Profile Fits to 20 March 1980 Observations

Station	Ring	Event	Midtime (UTC)	Width (km)	Equiv. Width E (km)	Equivalent Depth A (km)	Frac. Trans. f_0	Normal Optical Depth	True Anomaly (deg)
CTIO	α	E	5:00:59.639 ± 0.035	4.13 ± 0.12	[3.19]	6.11 ± 1.51	[0.23]	[1.48]	37.8
CTIO	β	I	4:32:32.516 ± 0.047	5.91 ± 0.27	[2.84]	3.91 ± 0.68	[0.51]	[0.66]	339.6
CTIO	γ	E	5:18:35.839 ± 0.011	3.32 ± 0.10	[2.75]	5.88 ± 1.69	[0.17]	[1.77]	38.4
CTIO	δ	E	5:21:19.991 ± 0.012	3.17 ± 0.12	[2.40]	4.49 ± 1.05	[0.24]	[1.42]	165.3
CTIO	ε	I	4:10:50.652 ± 0.008	22.12 ± 0.08					22.6
CTIO	ε	E	5:30:10.686 ± 0.006	28.27 ± 0.07					323.5
SAAO	α	I		7.72 ± 0.38					66.4
SAAO	γ	I		3.41 ± 0.51					88.7
SAAO	δ	I		5.67 ± 0.55					219.0
SAAO	ε	I		24.83 ± 0.63					27.7

Notes:
1) I and E stand for immersion and emersion, respectively.
2) Numbers in square brackets were derived from other parameters in the fit.

TABLE VII

Results of Ring Profile Fits to 15 - 16 August 1980 Observations

Station	Event	Ring	Midtime (UTC)	Width (km)	Equiv. Width E (km)	Equivalent Depth A (km)	Frac. Trans. f_0	Normal Optical Depth	True Anomaly (deg)
CTIO	6	E	00:46:00.280 ± 0.009	2.17 ± 0.19	[0.63]	0.75 ± 0.08	[0.69]	[0.35]	277.8
CTIO	5	E	00:46:52.178 ± 0.004	1.97 ± 0.07	[1.21]	1.99 ± 0.20	[0.33]	[1.01]	103.3
CTIO	4	E	00:47:33.061 ± 0.006	2.16 ± 0.11	[0.98]	1.34 ± 0.12	[0.51]	[0.62]	238.9
CTIO	α	E	00:51:53.291 ± 0.007	9.92 ± 0.12	[4.70]	6.60 ± 0.52	[0.49]	[0.67]	189.5
CTIO	β	E	00:53:43.798 ± 0.010	11.37 ± 0.18	[3.08]	3.64 ± 0.25	[0.71]	[0.32]	131.1
CTIO	η	E	00:56:42.933 ± 0.006	1.36 ± 0.19	[0.61]	0.84 ± 0.10	[0.51]	[0.62]	128.2
CTIO	γ	E	00:57:36.621 ± 0.003	3.68 ± 0.05	[3.17]	9.26 ± 2.51	[0.06]	[2.52]	267.0
CTIO	δ	E	00:58:56.628 ± 0.003	3.09 ± 0.07	[2.26]	4.51 ± 0.59	[0.20]	[1.46]	48.2
CTIO	ε	I	21:52:54.950 ± 0.009	31.35 ± 0.17					49.1
CTIO	ε	E	01:04:45.902 ± 0.006	67.71 ± 0.09	[46.70]	86.64 ± 9.60	[0.25]	[1.28]	256.5
ESO	6	I	22:11:16.732 ± 0.012	(0.85 ± 0.61)	[0.55]	0.97 ± 0.38	[0.28]	[1.14]	63.8
ESO	6	E	00:45:58.387 ± 0.009	1.99 ± 0.20	[0.63]	0.77 ± 0.06	[0.66]	[0.39]	277.9
ESO	5	I	22:10:21.168 ± 0.009	1.45 ± 0.25	[0.95]	1.73 ± 0.25	[0.26]	[1.20]	249.7
ESO	5	E	00:46:50.316 ± 0.008	1.84 ± 0.18	[1.28]	2.36 ± 0.27	[0.25]	[1.28]	103.5
ESO	4	I	22:09:50.397 ± 0.010	1.04 ± 0.52	[0.67]	1.19 ± 0.31	[0.28]	[1.15]	25.6
ESO	4	E	00:47:31.222 ± 0.011	2.08 ± 0.22	[1.04]	1.51 ± 0.16	[0.46]	[0.72]	239.1
ESO	α	I	22:05:25.188 ± 0.007	2.70 ± 0.12	[2.35]	8.62 ± 2.59	[0.03]	[3.19]	337.8
ESO	α	E	00:51:51.697 ± 0.013	10.01 ± 0.23	[4.71]	6.60 ± 0.41	[0.49]	[0.66]	189.6
ESO	β	I	22:03:27.298 ± 0.014	5.71 ± 0.25	[2.58]	3.59 ± 0.28	[0.50]	[0.63]	280.1
ESO	β	E	00:53:42.363 ± 0.015	11.90 ± 0.26	[3.30]	3.93 ± 0.21	[0.70]	[0.33]	131.2
ESO	η	I	22:00:23.210 ± 0.030	2.82 ± 0.68	[0.44]	0.48 ± 0.08	[0.83]	[0.17]	278.2
ESO	η	E	00:56:41.676 ± 0.007						128.3
ESO	γ	I	21:59:28.651 ± 0.005	1.21 ± 0.22					57.4
ESO	γ	E	00:57:35.399 ± 0.005	3.66 ± 0.10	[3.24]	10.92 ± 2.19	[0.04]	[2.98]	267.1
ESO	δ	I	21:58:07.179 ± 0.008	3.73 ± 0.19	[2.49]	4.56 ± 0.41	[0.25]	[1.22]	199.0
ESO	δ	E	00:58:55.486 ± 0.010	2.95 ± 0.22	[2.28]	4.96 ± 0.75	[0.16]	[1.68]	48.3
ESO	ε	E	01:04:44.975 ± 0.007	67.70 ± 0.11	[47.14]	88.45 ± 5.02	[0.24]	[1.31]	256.6
LCO	6	E		1.99 ± 0.43	[0.63]	0.77 ± 0.16	[0.66]	[0.39]	277.9
LCO	5	E		1.79 ± 0.35	[1.14]	1.92 ± 0.42	[0.31]	[1.07]	103.5
LCO	4	E		2.14 ± 0.40	[1.02]	1.43 ± 0.29	[0.48]	[0.67]	239.1
LCO	α	I		4.83 ± 0.92	[3.32]	6.33 ± 2.40	[0.23]	[1.31]	337.8
LCO	α	E		9.70 ± 0.39	[4.48]	6.21 ± 0.59	[0.50]	[0.64]	189.6
LCO	β	I		6.90 ± 1.45	[3.44]	5.03 ± 1.90	[0.44]	[0.73]	280.0
LCO	β	E		10.72 ± 0.46	[3.05]	3.65 ± 0.34	[0.69]	[0.34]	131.2
LCO	η	E		1.44 ± 0.45	[0.72]	1.04 ± 0.29	[0.45]	[0.72]	128.3
LCO	γ	E		3.43 ± 0.36	[2.89]	7.80 ± 2.17	[0.08]	[2.27]	267.2
LCO	δ	I		5.94 ± 0.98	[3.14]	4.76 ± 1.40	[0.41]	[0.80]	198.9
LCO	δ	E		3.14 ± 0.48	[2.15]	3.95 ± 0.91	[0.25]	[1.26]	48.3
LCO	ε	I		32.37 ± 0.59	[25.54]	62.33 ± 21.02	[0.12]	[1.93]	48.9
LCO	ε	E		67.87 ± 0.36	[45.24]	80.79 ± 8.55	[0.27]	[1.19]	256.7

Notes:
1) I and E stand for immersion and emersion, respectively.
2) Numbers in square brackets were derived from other parameters in the fit.

vations were made using two telescopes (Sicardy *et al.*, 1985). Only the 2-m telescope observations have been included here; the 1-m results are far noisier. Because of timing problems, *there is a systematic error of several seconds* in the midtimes for the OPMT observations given in Table IX. This will be discussed in more detail in Section III. The results of Jablonski and Barroso (1985) were not used in the present analysis.

1 May 1982. The occultation of KME15 was successfully observed from Mt. Stromlo under clear conditions. The observations, and results of profile fits to the data, are described by French *et al.* (1986a).

4 June 1982. Observations of the occultation of KME16 were successfully made from Mt. Palomar, at 2.2 μm. Analysis of these observations will be published elsewhere. Approximate midtimes, provided by Philip Nicholson as determined from high-resolution plots of the data, are given in Table X. These data were used in the refined orbit calculation in Section III.

3 March 1983. KME17 was occulted twice by the rings, once on 3 March 1983 and again on 25 March 1983. The first occultation (KME17a) was observed from Perth under poor conditions. An ε ring timing was obtained, which was useful for updating the prediction of the 25 March 1983 event (IAUC, 1983).

25 March 1983. The second occultation of KME17 was successfully observed at 2.2 μm from SAAO. The observations and results of profile fits will be published elsewhere.

4 and 24 May 1985. The 4 and 24 May 1985 occultations of KME23 and KME25 were successfully observed by a worldwide network of observers (French *et al.*, 1985). To the best of our knowledge, these are the only Earth-based occultation observations of the rings since the 25 March 1983 event. The KME23 and KME25 data were obtained too recently for use in the present analysis.

III. URANIAN RING ORBITS

A. *Orbital Elements of the Rings*

The most recent determination of the orbital elements of the Uranian rings revealed that many of the rings have measureable

TABLE VIII

Results of Ring Profile Fits to 26 April 1981 Observations

Station	Ring	Event	Midtime (UTC)	Width (km)	Equiv. Width E (km)	Equivalent Depth A (km)	Frac. Trans. f_0	Normal Optical Depth	True Anomaly (deg)
AAT	6	I	19:18:56.572 ± 0.004	1.15 ± 0.43	[0.59]	0.85 ± 0.33	[0.47]	[0.74]	302.6
AAT	6	E	20:17:50.424 ± 0.006	2.23 ± 0.27	[0.49]	0.55 ± 0.08	[0.77]	[0.25]	73.2
AAT	5	I	19:18:31.020 ± 0.001	1.81 ± 0.22	[1.32]	2.46 ± 0.42	[0.25]	[1.36]	151.0
AAT	5	E	20:18:11.012 ± 0.004	2.71 ± 0.14	[1.26]	1.73 ± 0.20	[0.51]	[0.64]	282.1
AAT	4	I	19:18:19.237 ± 0.002	1.55 ± 0.33	[0.95]	1.49 ± 0.35	[0.37]	[0.96]	305.2
AAT	4	E	20:18:27.738 ± 0.003	2.89 ± 0.18	[1.11]	1.42 ± 0.14	[0.59]	[0.49]	76.7
AAT	α	I	19:16:30.501 ± 0.002	3.84 ± 0.09	[3.13]	6.86 ± 1.10	[0.16]	[1.78]	0.2
AAT	α	E	20:20:18.772 ± 0.004	10.82 ± 0.18	[4.61]	6.15 ± 0.49	[0.55]	[0.57]	134.2
AAT	β	I	19:15:42.376 ± 0.003	4.70 ± 0.13	[2.92]	4.67 ± 0.46	[0.36]	[0.99]	340.8
AAT	β	E	20:21:05.733 ± 0.006	11.64 ± 0.25	[3.46]	4.16 ± 0.36	[0.68]	[0.36]	115.8
AAT	η	I	19:14:25.460 ± 0.004	2.89 ± 0.28	[0.88]	1.06 ± 0.11	[0.68]	[0.37]	33.5
AAT	η	E	20:22:21.595 ± 0.007	1.37 ± 0.48	[0.56]	0.74 ± 0.26	[0.56]	[0.54]	170.0
AAT	γ	I	19:14:02.625 ± 0.001	3.27 ± 0.04	[3.03]	10.02 ± 3.74	[0.04]	[3.07]	187.3
AAT	γ	E	20:22:44.167 ± 0.003	3.90 ± 0.13	[2.73]	4.99 ± 0.76	[0.26]	[1.28]	324.3
AAT	δ	I	19:13:29.494 ± 0.002	3.85 ± 0.10	[2.73]	4.94 ± 0.60	[0.26]	[1.28]	349.8
AAT	δ	E	20:23:18.046 ± 0.008	6.89 ± 0.35	[3.03]	4.08 ± 0.50	[0.53]	[0.59]	127.4
AAT	ε	I	19:11:10.017 ± 0.002	55.38 ± 0.08	[44.41]	95.31 ± 13.57	[0.17]	[1.72]	274.9
AAT	ε	E	20:25:28.107 ± 0.002	34.05 ± 0.10	[28.19]	68.28 ± 12.40	[0.12]	[2.01]	54.9
Kavalur	ε	E		34.50 ± 1.98					49.0

Notes:
1) I and E stand for immersion and emersion, respectively.
2) Numbers in square brackets were derived from other parameters in the fit.

TABLE IX

Results of Ring Profile Fits to 22 April 1982 Observations

Station	Ring	Event	Midtime (UTC)	Width (km)	Equiv. Width E (km)	Equivalent Depth A (km)	Frac. Trans. f_0	Normal Optical Depth	True Anomaly (deg)
CTIO	6	I	1:42:41.517 ± 0.028		[0.79]	0.84 ± 0.42	[0.87]	[0.14]	25.2
CTIO	6	E	2:51:54.397 ± 0.009		[0.79]	0.86 ± 0.27	[0.85]	[0.16]	159.2
CTIO	5	I	1:42:15.747 ± 0.009		[1.27]	1.50 ± 0.40	[0.71]	[0.34]	266.2
CTIO	5	E	2:52:10.962 ± 0.014	4.04 ± 1.14	[1.08]	1.26 ± 0.21	[0.74]	[0.31]	40.5
CTIO	4	I	1:41:56.511 ± 0.015	3.20 ± 0.86	[0.98]	1.17 ± 0.28	[0.68]	[0.37]	86.8
CTIO	4	E	2:52:36.407 ± 0.016	4.90 ± 0.77	[1.12]	1.28 ± 0.15	[0.76]	[0.26]	221.6
CTIO	α	I	1:39:51.863 ± 0.007	6.48 ± 0.35	[3.47]	5.01 ± 0.27	[0.43]	[0.77]	290.6
CTIO	α	E	2:54:37.878 ± 0.007	8.16 ± 0.24	[4.42]	6.48 ± 0.29	[0.43]	[0.79]	67.6
CTIO	β	I	1:38:57.584 ± 0.011	6.04 ± 0.56	[2.43]	3.12 ± 0.22	[0.57]	[0.52]	326.9
CTIO	β	E	2:55:33.067 ± 0.013	11.37 ± 0.39	[3.48]	4.18 ± 0.19	[0.68]	[0.37]	104.9
CTIO	η	I	1:37:29.005 ± 0.027		[0.55]	0.61 ± 0.19	[0.81]	[0.21]	99.0
CTIO	η	E	2:56:59.683 ± 0.021		[0.70]	0.81 ± 0.23	[0.75]	[0.27]	238.4
CTIO	γ	I	1:37:03.011 ± 0.005	6.24 ± 0.33	[3.80]	5.93 ± 0.36	[0.37]	[0.95]	274.1
CTIO	γ	E	2:57:25.143 ± 0.006	5.39 ± 0.49	[3.22]	5.03 ± 0.43	[0.36]	[0.93]	53.9
CTIO	δ	I	1:36:24.393 ± 0.010	4.90 ± 0.69	[1.86]	2.35 ± 0.25	[0.62]	[0.48]	107.0
CTIO	δ	E	2:58:04.128 ± 0.008	7.35 ± 0.32	[3.34]	4.51 ± 0.22	[0.54]	[0.61]	247.4
CTIO	ε	I	1:33:22.755 ± 0.007	88.42 ± 0.15	[55.29]	88.06 ± 3.48	[0.33]	[1.00]	141.6
CTIO	ε	E	3:00:40.038 ± 0.004	46.14 ± 0.13	[36.76]	77.33 ± 4.60	[0.16]	[1.68]	284.4
ESO	5	I	1:42:20.994 ± 0.020						266.3
ESO	5	E	2:52:12.071 ± 0.007	5.28 ± 0.66	[1.49]	1.77 ± 0.15	[0.71]	[0.34]	40.4
ESO	4	I	1:42:01.738 ± 0.025						86.9
ESO	4	E	2:52:37.507 ± 0.009	6.08 ± 0.68	[1.35]	1.53 ± 0.12	[0.77]	[0.25]	221.5
ESO	α	I	1:39:56.980 ± 0.007						290.7
ESO	α	E	2:54:39.078 ± 0.003	7.82 ± 0.15	[4.50]	6.86 ± 0.25	[0.40]	[0.88]	67.5
ESO	β	E	2:55:34.319 ± 0.009	11.42 ± 0.41	[3.51]	4.23 ± 0.21	[0.68]	[0.37]	104.8
ESO	η	E	2:57:00.992 ± 0.015	(1.14 ± 0.45)	[0.73]	1.21 ± 0.52	[0.33]	[1.07]	238.2
ESO	γ	I	1:37:08.018 ± 0.012						274.2
ESO	γ	E	2:57:26.440 ± 0.003	5.83 ± 0.39	[3.55]	5.61 ± 0.39	[0.37]	[0.96]	53.8
ESO	δ	I	1:36:29.366 ± 0.015						107.1
ESO	δ	E	2:58:05.407 ± 0.006	7.61 ± 0.35	[3.51]	4.77 ± 0.23	[0.52]	[0.63]	247.3
ESO	ε	I	1:33:27.642 ± 0.016	88.30 ± 0.56	[59.91]	101.62 ± 6.39	[0.31]	[1.15]	141.7
ESO	ε	E	3:00:41.508 ± 0.004	46.17 ± 0.16	[37.42]	81.24 ± 5.22	[0.16]	[1.76]	284.3
LCO	6	I	1:42:47.973 ± 0.033	8.97 ± 4.92	[0.96]	1.02 ± 0.48	[0.89]	[0.11]	25.4
LCO	6	E	2:51:55.599 ± 0.044	(7.97 ± 8.82)	[0.73]	0.77 ± 0.45	[0.90]	[0.85]	159.0
LCO	5	I	1:42:22.292 ± 0.011						266.3
LCO	5	E	2:52:12.168 ± 0.015						40.4
LCO	4	I	1:42:03.064 ± 0.021	(5.42 ± 5.05)	[1.08]	1.21 ± 0.49	[0.80]	[0.22]	87.0
LCO	4	E	2:52:37.686 ± 0.013	(4.36 ± 6.62)	[1.22]	1.44 ± 0.40	[0.71]	[0.33]	221.4
LCO	α	I	1:39:58.262 ± 0.006	4.75 ± 1.54	[3.17]	5.31 ± 1.14	[0.32]	[1.12]	290.7
LCO	α	E	2:54:39.235 ± 0.004	7.05 ± 0.79	[4.72]	8.04 ± 0.94	[0.31]	[1.14]	67.5
LCO	β	I	1:39:03.958 ± 0.009	6.35 ± 1.78	[2.83]	3.76 ± 0.68	[0.55]	[0.59]	327.0
LCO	β	E	2:55:34.468 ± 0.010	10.44 ± 1.44	[3.61]	4.47 ± 0.67	[0.64]	[0.43]	104.7
LCO	η	I	1:37:35.330 ± 0.037	2.94 ± 0.72	[0.46]	0.51 ± 0.38	[0.84]	[0.17]	99.1
LCO	η	E	2:57:01.130 ± 0.021	2.97 ± 0.72	[0.71]	0.81 ± 0.41	[0.75]	[0.27]	238.2
LCO	γ	I	1:37:09.264 ± 0.005	5.51 ± 1.13	[4.13]	7.80 ± 1.67	[0.24]	[1.42]	274.3
LCO	γ	E	2:57:26.623 ± 0.004	4.79 ± 1.22	[3.53]	6.66 ± 1.64	[0.24]	[1.39]	53.8
LCO	δ	I	1:36:30.617 ± 0.009	5.15 ± 2.31	[2.35]	3.16 ± 0.68	[0.54]	[0.61]	107.1
LCO	δ	E	2:58:05.643 ± 0.006	6.56 ± 1.25	[3.53]	5.16 ± 0.73	[0.44]	[0.79]	247.3
LCO	ε	I	1:33:28.843 ± 0.012	88.05 ± 1.26	[56.34]	91.01 ± 8.30	[0.35]	[1.03]	141.8
LCO	ε	E	3:00:41.719 ± 0.003	46.25 ± 0.36	[38.88]	90.91 ± 8.50	[0.13]	[1.97]	284.3
OPMT	5	I	(1:43:31.429 ± 0.010)	7.05 ± 0.35	[1.35]	1.50 ± 0.13	[0.81]	[0.21]	280.4
OPMT	4	I	(1:43:07.656 ± 0.005)	6.36 ± 0.33	[1.41]	1.59 ± 0.11	[0.78]	[0.25]	100.8
OPMT	α	I	(1:40:49.254 ± 0.002)	7.89 ± 0.09	[3.53]	4.70 ± 0.33	[0.55]	[0.60]	303.8
OPMT	α	E	(2:46:23.935 ± 0.006)	9.19 ± 0.23	[4.20]	5.70 ± 0.43	[0.53]	[0.62]	55.1
OPMT	β	I	(1:39:48.768 ± 0.002)	7.48 ± 0.13	[2.64]	3.26 ± 0.22	[0.64]	[0.44]	339.7
OPMT	γ	I	(1:37:43.050 ± 0.004)	7.08 ± 0.23	[2.75]	3.50 ± 0.25	[0.61]	[0.49]	286.3
OPMT	γ	E	(2:49:29.694 ± 0.007)	8.52 ± 0.29	[3.54]	4.62 ± 0.35	[0.57]	[0.54]	42.4
OPMT	δ	I	(1:37:00.978 ± 0.005)	8.29 ± 0.24	[2.23]	2.60 ± 0.17	[0.73]	[0.31]	119.0
OPMT	δ	E	(2:50:12.430 ± 0.005)	8.53 ± 0.16	[2.99]	3.72 ± 0.26	[0.64]	[0.44]	236.0
OPMT	ε	I	(1:33:42.421 ± 0.007)	93.54 ± 0.21	[60.95]	99.33 ± 9.37	[0.34]	[1.06]	152.7
OPMT	ε	E	(2:53:06.651 ± 0.002)	53.65 ± 0.07	[40.20]	77.23 ± 9.02	[0.23]	[1.44]	273.9

Notes:
1) I and E stand for immersion and emersion, respectively.
2) Numbers in square brackets were derived from other parameters in the fit.
3) OPMT midtimes have a systematic offset of several seconds. See text for details.

TABLE X

Adopted Midtimes for 4 June 1982 Observations from Palomar Observatory

Ring	Event	Midtime (UTC)
6	I	5:23:46.86
6	E	6:15:04.38
5	I	5:23:22.15
5	E	6:15:26.68
4	I	5:23:11.32
4	E	6:15:44.15
α	I	5:21:19.57
α	E	6:17:30.14
β	I	5:20:33.91
β	E	6:18:17.10
η	I	5:19:19.63
η	E	6:19:32.69
γ	I	5:18:57.23
γ	E	6:19:54.96
δ	I	5:18:24.77
δ	E	6:20:27.58
ε	I	5:16:07.12
ε	E	6:23:00.31

inclinations (French *et al.*, 1982; Elliot and Nicholson, 1984). Since then, additional occultations by the rings have been observed, and a revised set of event midtimes has been obtained from model fits to the ring profiles, as described in the previous section. With the availability of new data, and the necessity of determining accurate true anomalies for each ring event to refine the width–longitude relations of the rings, a new solution for the ring orbits seemed in order.

The steps in the fitting procedure are summarized by Elliot and Nicholson (1984). Details of the method are discussed by Elliot *et al.* (1978, 1981b) and French *et al.* (1982). We used only data which were recorded on magnetic tape (Table I), and we followed a two-step procedure in the fit. Using the newly derived midtimes, it was clear that the γ and δ rings had much larger residuals than the other rings. Therefore, we excluded the γ and δ ring data, and fitted the orbital elements of the other seven rings, as well as the direction of the planetary pole, the gravitational harmonics, J_2 and J_4, and corrections to the relative position of the planet and star for each occultation. Additionally, we fitted for an offset to the absolute timing for three stations (ESO for KM12, and ESO and LCO for KME14), since there appeared to be a systematic offset between the time base used by several observers. Having thus determined the geometry of the ring system from the "well-behaved" rings, we then fitted the γ and δ ring data alone for their orbital elements. The results are given in Table XI.

The midtimes used for the fits to the ring orbital elements have typical uncertainties of $\sigma(t_0) \simeq 0.015$ sec; for some rings, they are as low as 0.002 sec. (Tables III–X). The best previous ring orbit fit had residuals 10 times larger than this (Elliot and Nicholson, 1984), but the situation has improved dramatically in the present model. It is clear that a major source of error in earlier fits was the inclusion of midtimes estimated from strip chart records. We have plotted residuals in both ring plane radius (Δr) and time (Δt) for all data used in the new model fit in Fig. 1. The rms residuals in Δr and Δt are tabulated for each ring in Table XII.

Two points are immediately obvious. First, for most of the rings, typical radius residuals are only a few hundred meters. This is comparable to the uncertainty in the position of the KAO during the 10 March 1977 occultation, and the corresponding timing residuals are only slightly larger than $\sigma(t_0)$, indicating that, for these rings, any deviations from elliptical orbits are quite small. Second, the γ and δ rings clearly have residuals much larger than can be accounted for by uncertainties in midtimes, and roughly *10* times larger than residuals for the other rings. We will consider these two rings later.

It is important to recognize several limitations of these results. A number of effects that may ultimately be important have not been included in the model. In particular, there has been no correction for motion of the planet with respect to the system barycenter during an occultation, nor for the precession rates induced by the known Uranian satellites. Secondly, tests have shown that the results depend *critically* on the 22 April 1982 observations, which have by far the largest north–south coverage of any data sets used in the fit. The difficulty

TABLE XI

Fitted Model Parameters [a]

Ring	Semimajor Axis a (km)	Eccentricity e (x 10^3)	Longitude of Periapse ϖ_0 (deg) [b]	Inclination i (deg)	Longitude of Ascending Node Ω_0 (deg) [b]
6	41845.9 ± 4.6	1.001 ± 0.024	242.6 ± 2.1	0.0627 ± 0.0067	12.0 ± 3.6
5	42243.4 ± 4.9	1.900 ± 0.029	170.2 ± 1.8	0.0519 ± 0.0085	286.0 ± 5.0
4	42579.3 ± 4.8	1.065 ± 0.029	126.5 ± 1.8	0.0317 ± 0.0036	89.4 ± 12.5
α	44726.6 ± 4.9	0.759 ± 0.026	332.9 ± 1.5	0.0145 ± 0.0051	64.7 ± 16.0
β	45668.8 ± 5.0	0.438 ± 0.022	224.7 ± 4.0	0.0052 ± 0.0033	303.8 ± 71.7
η	47183.6 ± 5.2	(0.014 ± 0.025)	(143.0 ± 79.6)	(0.0023 ± 0.0032)	(243.8 ± 126.0)
γ [c]	47632.3 ± 5.1	(0.121 ± 0.201)	78.3 ± 64.1	(0.0106 ± 0.0314)	(4.3 ± 98.9)
δ [c]	48306.1 ± 4.7	(0.020 ± 0.140)	(42.8 ± 322.1)	0.0039 ± 0.0023	(315.3 ± 322.1)
ε	51156.3 ± 4.9	7.924 ± 0.023	214.8 ± 0.4	(0.0012 ± 0.0045)	(301.4 ± 327.3)

Harmonic Coefficients of the Gravity Potential [d]	Pole of the Equatorial Plane
$J_2 = (3.3461 \pm 0.0030) \times 10^{-3}$	α (1950.0) $5^h\ 06^m\ 25.6^s \pm 4.6^s$
$J_4 = (-3.21 \pm 0.37) \times 10^{-5}$	δ (1950.0) +15° 01′ 56″ ± 2′ 09″

Corrections to the Relative Positions of Uranus and Occulted Stars

		Adopted Stellar Coordinates (1950.0) [e]		Corrections [f]	
Date	Star	α	δ	α	δ
10 Mar. 1977	SAO 158687	$14^h\ 35^m\ 26.8930^s$	-14° 44′ 20.570″	-0.0215[s]	-0.302″
10 Apr. 1978	KM5	$14^h\ 50^m\ 37.8100^s$	-15° 56′ 59.800″	-0.0508[s] [g]	-0.172″ [g]
10 June 1979	KM9	$14^h\ 59^m\ 58.1000^s$	-16° 41′ 29.700″	-0.0305[s] [g]	+0.241″ [g]
20 Mar. 1980	KM11	$15^h\ 30^m\ 46.4300^s$	-18° 44′ 02.600″	-0.0147[s] [g]	-0.408″ [g]
15 Aug. 1980	KM12	$15^h\ 15^m\ 19.9100^s$	-17° 48′ 46.400″	-0.0167[s]	-0.136″
26 Apr. 1981	KME13	$15^h\ 45^m\ 31.7730^s$	-19° 37′ 16.960″	-0.0200[s]	-0.108″
22 Apr. 1982	KME14	$16^h\ 05^m\ 39.7820^s$	-20° 40′ 33.060″	-0.0121[s]	-0.200″
1 May 1982	KME15	$16^h\ 04^m\ 14.5090^s$	-20° 36′ 42.980″	-0.0052[s]	-0.244″
4 June 1982	KME16	$15^h\ 58^m\ 32.7180^s$	-20° 20′ 57.540″	-0.0130[s]	+0.036″
25 Mar. 1983	KME17b	$16^h\ 27^m\ 33.0040^s$	-21° 38′ 03.850″	-0.0186[s]	-0.127″

Fitted Time Offsets

Date	Station	Offset (s)
15 Aug. 1980	ESO	0.051 ± 0.081
22 Apr. 1982	ESO	-0.147 ± 0.064
22 Apr. 1982	LCO	-0.025 ± 0.058

(a) For $M = 8.669 \times 10^{28}$ gm and $G = 6.670 \times 10^{-8}$ dyne cm^2 gm^{-2}, which combined give $GM = 5.782223 \times 10^{21}$ cm^3 gm^{-1} sec^{-2}. See text for discussion of errors.
(b) At 20:00 UT on 10 March 1977.
(c) γ and δ rings were fitted separately. See text for details.
(d) For a reference radius R = 26,200 km.
(e) Stellar positions from Klemola (1985) for SAO 158687, and Klemola and Marsden (1977) and Klemola *et al.* (1981) for the other occulted stars.
(f) planet - star position (observed - predicted) at the time of the occultation, using the DE-118 ephemeris for Uranus (Standish, 1982) and a Perth 70 reference system for the stars [see note (e)]. Estimated uncertainty of the corrections is ± 0.002".
(g) Corrections for these events were determined separately, on the basis of the standard ring orbit solution and approximate event times determined from ring profile fits to digitized strip chart data. See text for details.

here is that the OPMT observations are known to have a systematic timing error of several seconds, and that, even when this is taken into account, these observations are not compatible with the Tenerife observations, which were recorded on different tapes, with different clock settings, for immersion and emersion. For the fit results given here, we have excluded the OPMT results and included the Tenerife results. If we had made the opposite choice, a number of fitted parameters would change by more than their formal errors. *The error bars given in Table XI are five times the formal errors*, in order to reflect more realistically the consequent uncertainty in these orbital elements. (This value was chosen on the basis of trial model fits, using subsets of the full data set.) Barring an independent

TABLE XII

Ring Orbit Residuals (rms)

Ring	Radius Δr (km)	Time Δt (sec)
6	0.59	0.034
5	0.22	0.015
4	0.27	0.016
α	0.18	0.012
β	0.31	0.022
η	0.55	0.032
γ	3.35	0.194
δ	2.69	0.179
ε	0.52	0.028

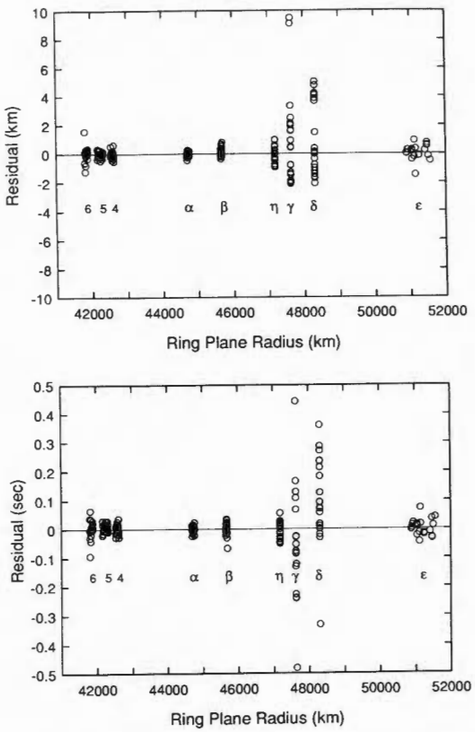

FIG. 1. Residuals of a fit to ring midtimes, assuming a model of uniformly precessing, inclined, elliptical rings. The upper figure shows post-fit residuals in ring plane radius, Δr, plotted vs ring plane radius. The lower figure shows the residuals in time, Δt. The γ and δ rings have residuals much larger than can be accounted for by random errors in the fitted midtimes.

means of determining which of the two data sets might be in error, we caution that the fitted values of Tables XI and XII are based on the assumption that there are no systematic timing errors in the Tenerife data. This subject is discussed in more detail by Millis *et al.* (1986). When *both* the OPMT and Tenerife observations were omitted from the fit, the formal errors increased substantially. The lessons are that accurate absolute timing is essential if we are to have confidence in the orbit results at the level of the formal errors, and that long north–south baselines substantially reduce the errors. Global observations of two occultations in May 1985 were recently carried out for this reason (French *et al.*, 1985). We anticipate that the ring orbital elements will be even more accurately known when these data are included in the orbit model.

We note for comparison that Veillet (1983) determined the pole of the plane of Titania, Umbriel, and Ariel to be $\alpha(1950.0) = 5^h07^m00.2^s \pm 5.8^s$, $\delta(1950.0) = +15°03'58'' \pm 1'48''$, compared to our values of $\alpha(1950.0) = 5^h06^m25.6^s \pm 4.6^s$ and $\delta(1950.0) = +15°01'56'' \pm 2'09''$. If the difference in $\alpha(1950.0)$ is real, it may represent an interesting dynamical effect, although Dermott and Nicholson (1986) have called into question some of Veillet's results. As an additional note of caution we mention that our present determination of the pole direction differs appreciably from the previous published model (Elliot and Nicholson, 1984). The difference can be traced to three factors: (1) the exclusion of strip chart data from the present fit; (2) the exclusion of γ and δ ring data in the fit used to determine the pole direction; and (3) the inclusion of the Tenerife data of the occultation of KME14. With the inclusion of additional observations, it should become clear if the current pole determination is accurate.

Eshleman *et al.* (1983) proposed an alternative model for the kinematics of narrow planetary rings, involving entwined particle orbits. The apsidal precession and nodal regression rates of the Uranian rings are not compatible with their model, and we have not been able to obtain good fits to the data, using their predicted precession and regression conditions.

B. Limits on Shepherd Satellites

The presence of small shepherd satellites in the vicinity of the Uranian rings has been proposed to account for the confinement of ring material (Goldreich and Tremaine, 1979a). If the shepherds were large enough, they would produce noticeable forced precessions in the rings, as well as measurable perturbations of the ring shapes from ellipses. These effects have been evaluated quantitatively for the Uranian system by

Freedman *et al.* (1983). By examining the post-fit residuals of the present orbit model (Fig. 1), we are now able to place stringent limits on the properties of shepherd satellites that might be present.

The characteristic amplitude of forced radial oscillations, Δr, due to a shepherd satellite of mass m, orbiting at a radius r, near a circular ring of radius a is (Freedman *et al.*, 1983)

$$|\Delta r| = 3 \text{ km} \left(\frac{m}{10^{19} \text{ g}}\right) \left(\frac{r}{50{,}000 \text{ km}}\right)^3 \left(\frac{100 \text{ km}}{a - r}\right)^2. \quad (1)$$

For $|\Delta r| = 0.3$ km, a typical value for the well-behaved rings (Table XII), we find

$$m < 10^{18} \text{ g} \left(\frac{a - r}{100 \text{ km}}\right)^2, \quad (2)$$

corresponding to a shepherd diameter, d, given by

$$d < \frac{12 \text{ km}}{\rho^{1/3}} \left(\frac{a - r}{100 \text{ km}}\right)^{2/3}, \quad (3)$$

where ρ is the density of the shepherd satellite (in g cm^{-3}). These limits are only approximate, since oscillations in the rings may be damped before they have traveled very far from the perturbing satellite. This is discussed in detail by Cuzzi and Scargle (1985). Figure 2a shows the mass limits of Eq. (1) for a range of radial perturbations, Δr, comparable to the observational limits of Table XII.

Another method of determining shepherd satellite properties is to search for anomalous precession rates for the rings with measurable eccentricities. We fitted the data with the apsidal precession and nodal regression rates ($\dot{\varpi}$ and $\dot{\Omega}$) of the elliptical and inclined rings as free parameters

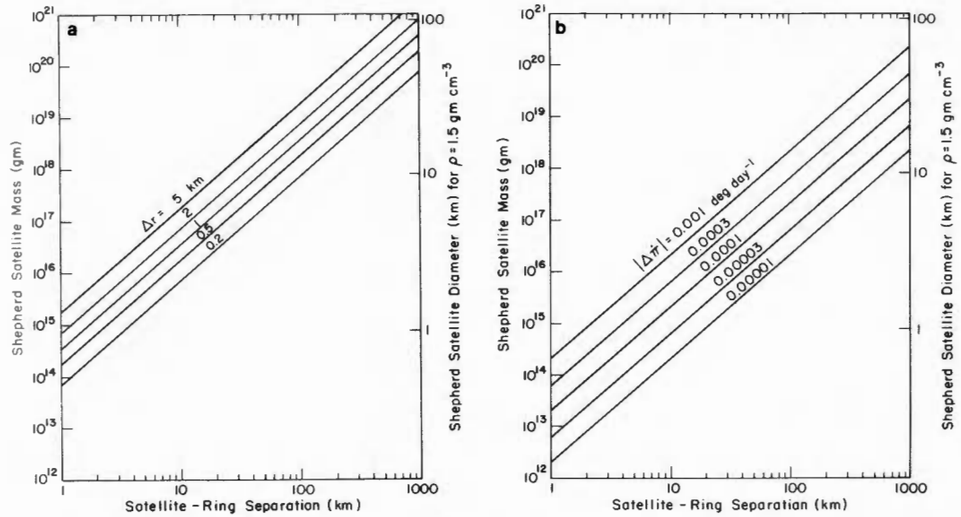

FIG. 2. (a) Limits on shepherd satellite masses, as a function of distance between the shepherd and the ring, for a range of rms radial perturbation amplitudes Δr. The satellite diameter is also given, for an assumed density of 1.5 g cm^{-3}. Post-fit residuals give $\Delta r = 0.2$–0.6 km for all but the γ and δ rings, for which $\Delta r \simeq 3$ km. (See Table XII.) (b) Limits on shepherd satellite masses, as a function of distance between the shepherd and the ring, for a range of anomalous precession rates, $|\Delta\dot{\varpi}|$. The satellite diameter is also given, for an assumed density of 1.5 g cm^{-3}. Individual fits to the eccentric rings give upper limits to anomalous apsidal precession rates of order 10^{-4} deg day^{-1}. (See Table XIII for detailed results.)

(rather than being determined from J_2 and J_4), along with the other orbital elements. The values for $\dot{\tilde{\pi}}$ and $\dot{\Omega}$ so obtained are compared to the rates calculated from J_2 and J_4 in Table XIII. The differences, $\Delta\dot{\tilde{\pi}}$ and $\Delta\dot{\Omega}$, bracketed by their error bars, represent upper limits to the anomalous precession and regression rates induced by shepherd satellites.

Since the precession rates are known more accurately than the regression rates (owing to the small inclinations of the rings and the current face-on geometry of the ring system), we will use the precession rate results to place limits on shepherd satellites. (For simple models of shepherd interactions, we expect $\Delta\dot{\tilde{\pi}} = -\Delta\dot{\Omega}$.) Freedman *et al.* (1983) find

$$\Delta\dot{\tilde{\pi}} = \frac{-1}{2\pi}\left(\frac{GM}{r^3}\right)^{1/2}\left(\frac{m}{M}\right)\left(\frac{a}{a-r}\right)^2, \quad (4)$$

where G is Newton's constant and M is the mass of Uranus. Numerically,

$$m < 2 \times 10^{17}\ \mathrm{g}\left(\frac{|\Delta\dot{\tilde{\pi}}|}{0.0001\ \mathrm{deg\ day^{-1}}}\right)\left(\frac{a-r}{100\ \mathrm{km}}\right)^2. \quad (5)$$

For $|\Delta\dot{\tilde{\pi}}| = 0.0002$ deg day^{-1}, a typical value (see Table XIII), the limits on the shepherd mass and radius are

$$m < 4 \times 10^{17}\ \mathrm{g}\left(\frac{a-r}{100\ \mathrm{km}}\right)^2 \quad (6)$$

and

$$d < \frac{9\ \mathrm{km}}{\rho^{1/3}}\left(\frac{a-r}{100\ \mathrm{km}}\right)^{2/3}, \quad (7)$$

comparable to the results found from radial perturbations [Eqs. (2) and (3)]. These results are shown in Fig. 2b for a range of anomalous precession rates comparable to the observational limits of Table XIII. If a shepherd satellite resides midway between two typical rings and has $\rho \simeq 1$ g cm^{-3}, its diameter d could be as large as 15 km. This would be detectable in images taken during the January 1986 Voyager encounter unless the satellite had a very low albedo, similar to the ring material (Miner *et al.*, 1985). According to P. Goldreich (private communication, 1985), even such small satellites are capable of confining narrow rings.

Since the rms radial perturbation, Δr, and the forced precession rate $\Delta\dot{\tilde{\pi}}$ have the same dependence on $(a - r)$, Eqs. (1) and (5) can be combined to give a simple relation between these two quantities:

$$\Delta r\ (\mathrm{km}) = 0.06\left(\frac{r}{50{,}000\ \mathrm{km}}\right)^3 \frac{|\Delta\dot{\tilde{\pi}}|}{0.0001\ \mathrm{deg\ day^{-1}}}. \quad (8)$$

Since the actual radial perturbations depend on the damping characteristics of the ring, whereas $\Delta\dot{\tilde{\pi}}$ does not, the limits on the shepherd masses using $\Delta\dot{\tilde{\pi}}$ may ultimately be more reliable than those using Δr. On the other hand, these conclusions strictly apply only to near-circular orbits for both ring and satellite [i.e., for $ae \ll |a(\mathrm{ring}) - a(\mathrm{sat})|$]. If this inequality is not satisfied, as it well may not be for close shepherds, then the more complicated results of Borderies *et al.* (1983a) must be used. It is even possible for the sign of the induced precession to change, if $e(\mathrm{ring}) < e(\mathrm{sat})$.

TABLE XIII

Precession and Regression Rates

Ring	Apsidal Precession Rate (deg day^{-1}) from J_2, J_4	fit	difference	Nodal Regression Rate (deg day^{-1}) from J_2, J_4	fit	difference
6	2.76182	2.76155 ± 0.00039	0.00027	-2.75644	-2.75809 ± 0.00119	0.00162
5	2.67148	2.67148 ± 0.00016	0.00000	-2.66637	-2.66520 ± 0.00069	-0.00117
4	2.59805	2.59819 ± 0.00046	-0.00014	-2.59316	-2.59225 ± 0.00273	-0.00091
α	2.18522	2.18554 ± 0.00112	-0.00032	-2.18149	-2.18280 ± 0.00742	0.00131
β	2.03078	2.03016 ± 0.00105	0.00062	-2.02745	-2.05468 ± 0.01312	0.02723
ε	1.36316	1.36318 ± 0.00003	-0.00002	-1.36138	(a)	(a)

(a) The ε ring does not have a discernable inclination (see Table XI).

C. *Perturbations of the γ and δ Rings*

It is tempting to regard the large residuals in the γ and δ rings ($\Delta r \simeq 3$ km, Table XII) as *prima facie* evidence for the existence of shepherd satellites near these rings. If a single large satellite midway between the γ and δ rings were responsible for the radial perturbations, its mass would be $m \simeq 10^{20}$ g [Eqs. (1) and (2)], with a diameter $d \simeq 50$ km for $\rho = 1$ g cm^{-3}. Such a large satellite would be easily visible in Voyager images, but it would also be large enough to produce radial perturbations in the nearby η ring of $\Delta r \simeq 0.4$ km. Indeed, in Table XII and Fig. 1, the η ring does appear to have somewhat larger residuals than the other "well-behaved" rings. The larger residuals may be due to the fact that the η ring profiles generally have low *S/N*, and therefore their fitted midtimes have greater uncertainties than the other rings.

It is also possible that smaller shepherd satellites, quite near to the γ and δ rings, are responsible for the observed perturbations, but there is some evidence that this is not the case. In the simple case of a shepherd in a circular orbit near a circular ring, the induced perturbation in the ring is roughly sinusoidal with a wavelength $\lambda = 3\pi|a - r|$ [see Cuzzi and Scargle (1985) for a heuristic derivation]. Thus, the *longest* azimuthal wavelength expected in the γ and δ rings, due to a shepherd midway between them, would be $\lambda \simeq 3200$ km.

The 22 April 1982 occultation of KME14 was observed from widely separated stations in the Northern and Southern Hemispheres, making it possible to map the ring orbit residuals, Δr, of the γ and δ rings, both for immersion and for emersion, over distances of more than 8000 km. The results are shown in Figs. 3 and 4, using the ring orbit model of Table XI. (A constant timing offset was fitted for the OPMT data plotted in these figures.) Shepherd satellites near the γ and δ rings could produce radial perturbations of the required magnitude, but the azimuthal wavelength would be less than about 3200 km (about 4° of ring longitude), whereas the systematic trends in Figs. 3 and 4 suggest (but do not prove) that the radial perturbations have a much larger wavelength—in excess of 10^4 km.

This has prompted us to examine other possible mechanisms for producing ring perturbations of low azimuthal wavenumber. For example, a Lindblad resonance with a small satellite inside the orbit of Miranda could give rise to radial perturbations of the form $\Delta r(\theta) = A\cos(m\theta)$, where

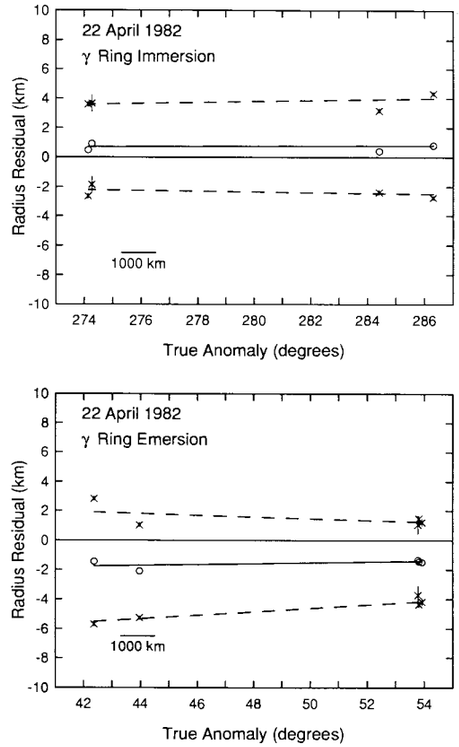

FIG. 3. Radius residuals from the orbit model fit to the γ ring (Table XI) as a function of true anomaly for the observations of 22 April 1982. The circles correspond to the post-fit ring-plane radius residuals. They are bracketed by pluses (with error bars) showing the measured ring edges with the vertical bar of each plus giving the uncertainty for each profile. The dashed lines are linear interpolations, schematically indicating possible locations of the inner and outer edges for the unobserved true anomalies of the rings, and the solid line represents a plausible midline of the ring.

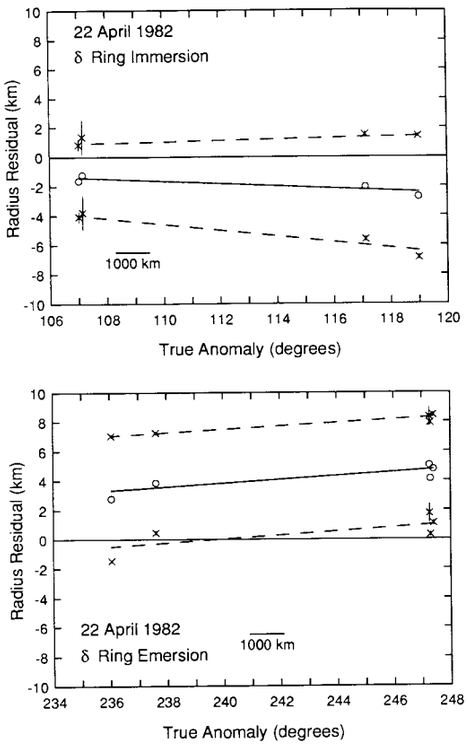

FIG. 4. Radius residuals from the orbit model fit to the δ ring (Table XI) as a function of true anomaly for the observations of 22 April 1982. The circles correspond to the post-fit ring-plane radius residuals. They are bracketed by pluses (with error bars) showing the measured ring edges with the vertical bar of each plus giving the uncertainty for each profile. The dashed lines are linear interpolations, schematically indicating possible locations of the inner and outer edges for the unobserved true anomalies of the rings, and the solid line represents a plausible midline of the ring.

the amplitude A depends on the satellite's mass and the location of the resonance, m is the azimuthal wavenumber, and θ is the ring longitude measured with respect to the satellite position. A number of resonances of this form are important in the Saturn ring system (Porco *et al.*, 1984a, 1984b). Another possibility is that normal modes are excited by a viscous instability in the rings. This mechanism has been investigated by Borderies *et al.* (1985), using a model for dense rings derived from studies of grain flow. The results of our analysis are given in French *et al.* (1986b), where we present evidence of a 2 : 1 Lindblad resonance associated with the δ ring.

IV. WIDTHS OF THE RINGS

A. *Width–Longitude Relations*

Prior to the discovery of the Uranian rings, it was conventional wisdom that planetary rings must necessarily be circular, because differential precession across an eccentric ring would soon lead to particle collisions that would circularize the ring. Since many rings in both the Uranus and Saturn systems are manifestly eccentric, there must be some mechanism to prevent this rapid circularization. Nicholson *et al.* (1978) demonstrated that the ε ring undergoes locked precession, and Goldreich and Tremaine (1979b) proposed that the self-gravity of the ring provided the torques necessary to prevent differential precession. Since then, the α and β rings have been shown to undergo locked precession (Elliot *et al.*, 1981a; Nicholson *et al.*, 1982; Elliot and Nicholson, 1984), as have several of Saturn's narrow ringlets (Porco *et al.*, 1984a, 1984b).

If the inner and outer edges of a ring are ellipses that precess uniformly, then the ring width, W, varies with true anomaly θ, as

$$W = r(a + \delta a/2,\ e + \delta e/2,\ \theta - \delta\tilde{\omega}/2) - r(a - \delta a/2,\ e - \delta e/2,\ \theta + \delta\tilde{\omega}/2), \quad (9)$$

where $r(a, e, \theta) = a(1 - e^2)/(1 + e\cos\theta)$; δa is $(1 - e^2)$ times the width of the ring at quadrature; δe is the differential eccentricity across the ring [in the sense (outer edge-inner edge)]; $\delta\tilde{\omega}$ is the angle between the lines of apsides of the outer and inner ring edges; and a and e are the mean semimajor axis and eccentricity of the ring as determined from the orbit solution to ring midtimes. From Eq. (9), it can be shown that, for $\delta\tilde{\omega}$ small, the width of a ring will vary linearly with the orbital radius.

With the availability of accurate ring widths (and their errors) for all of the rings, it is now possible to refine the width–longitude relations for the α, β, and ε rings and to determine whether the other rings have simple width–longitude relations as well. We fitted Eq. (9) to the width data for all rings, and obtained the results shown in Figs. 5–7 and tabulated in Table XIV.

For the α, β, and ε rings (Fig. 5), we performed unweighted fits to the data and included δa, δe, and $\delta\tilde{\omega}$ as free parameters. For both the α and β rings, there is a measurable apsidal twist (i.e., $\delta\tilde{\omega} \neq 0$), which can be related to dissipative mechanisms in the rings, as discussed in Section V. From Fig. 5 it is clear that there are significant deviations from the simple sinusoidal variation predicted by Eq. (9). As an extreme example, the α ring widths obtained from the KAO observation of 10 March 1977 are 7.72 ± 0.24 km for $\theta = 178.7°$ and 9.41 ± 0.21 km for $\theta = 65.9°$: the ring appears to be narrower at the larger orbital radius (see circled points in Fig. 5). These deviations cannot be attributed to an inclination gradient across the ring, which even in the most extreme case would account for a fractional width change of only a few percent, far less than the observed scatter. (A complicating factor in the interpretation is that the α ring sometimes shows a double-dip structure, evidence of nonuniform radial structure.)

Rings 6, 5, and 4 have measurable eccentricities, but nevertheless do not appear to

TABLE XIV

Results of Width-Longitude Fits					
Ring	δa (km)	δe (x 10^5)	δω̃ (deg)	ΔW(km)	$\frac{\Delta r}{\Delta W}$
6	1.84 ± 0.18	-0.9 ± 0.8	(0.0)	0.50	1.18
5	3.38 ± 0.43	-3.6 ± 1.8	(0.0)	1.61	0.14
4	3.37 ± 0.43	2.3 ± 1.7	(0.0)	1.80	0.15
α	7.39 ± 0.31	5.8 ± 1.0	-2.2 ± 0.7	1.40	0.13
β	8.79 ± 0.21	5.8 ± 0.8	-5.2 ± 0.9	0.95	0.33
η	2.41 ± 0.23	-1.0 ± 0.8	(0.0)	0.72	0.76
γ	4.16 ± 0.48	-1.1 ± 1.8	(0.0)	1.79	1.87
δ	5.14 ± 0.44	2.1 ± 1.4	(0.0)	1.99	1.35
ε	58.06 ± 0.26	74.9 ± 0.8	-0.01 ± 0.05	1.42	0.37

Notes:
1) Quantities in parentheses were held fixed during the fits.
2) ΔW is the rms post-fit width residual.
3) Δr is the rms post-fit ring radius residual from the orbit model.

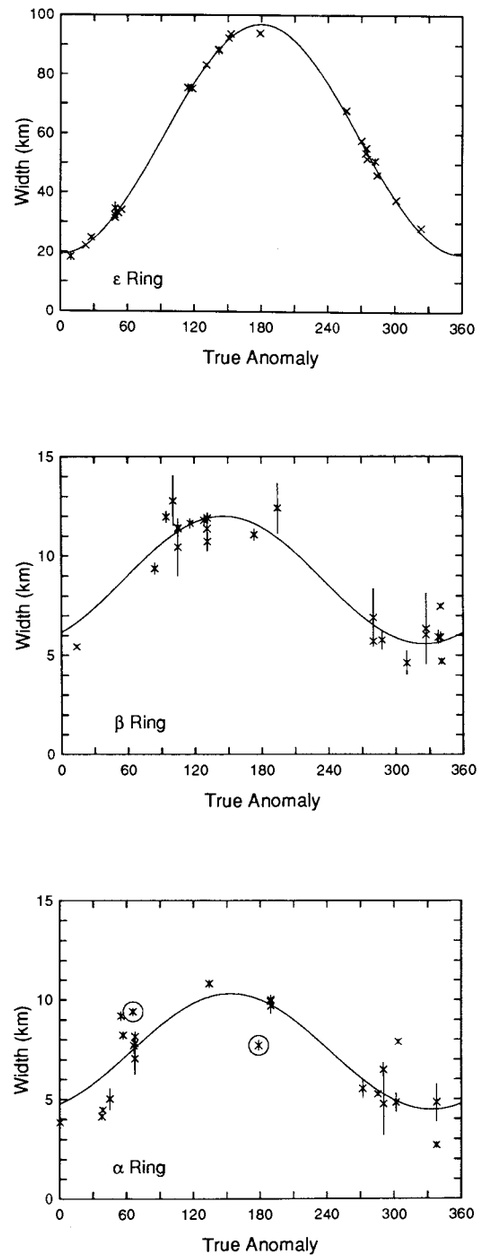

FIG. 5. Ring width vs true anomaly for the ε, β, and α rings. For each ring, an unweighted fit was performed for δa, δe, and $\delta\tilde{\omega}$. There are significant deviations from the best fitting simple sinusoidal variation. See text for discussion of the two circled α ring points.

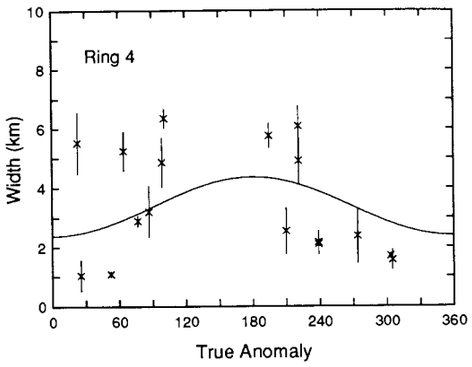

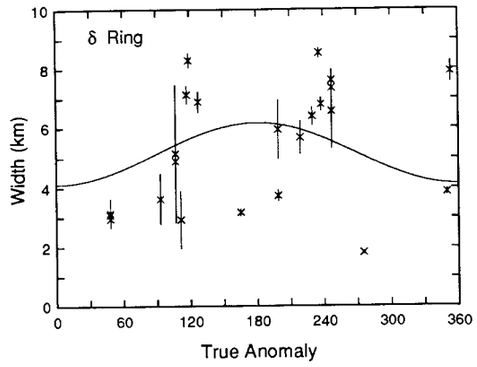

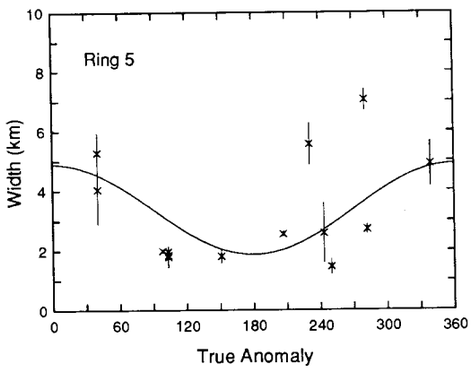

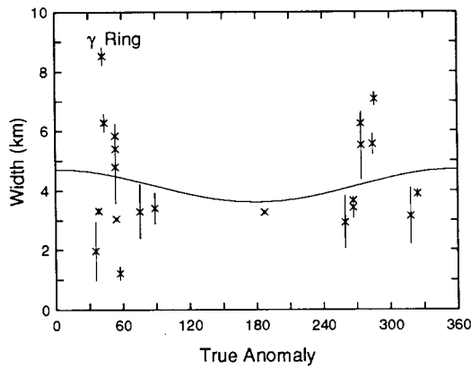

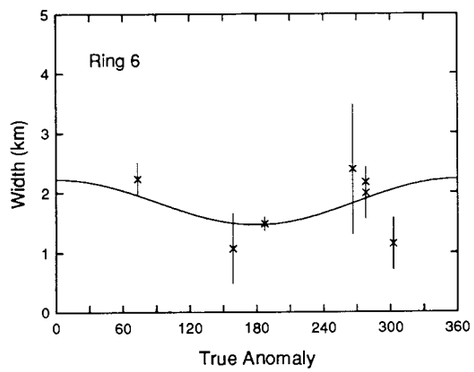

FIG. 6. Ring width vs true anomaly for rings 4, 5, and 6. The best-fitting solution for δa and δe is shown. The observations cannot be matched by a simple width–longitude relation, even though all three rings have well-determined eccentricities.

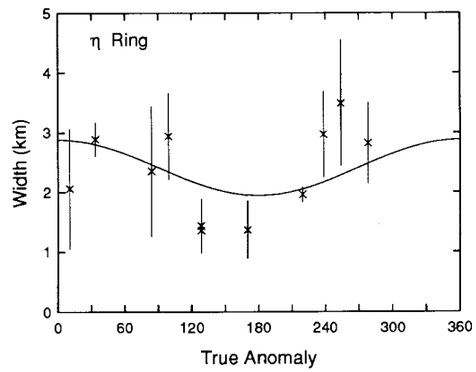

FIG. 7. Ring width vs true anomaly for rings δ, γ, and η. The best-fitting solution for δa and δe is shown. The observations cannot be matched by a simple width–longitude model.

have simple width–longitude relations (Fig. 5). For these data, we performed unweighted fits and held $\delta\tilde{\omega}$ fixed at zero. There is no trace of a sinusoidal variation in ring width with true anomaly for these rings. Whether the width perturbations are due to shepherd satellites is not known.

Rings η, γ, and δ are quasi-circular, and might be expected to have constant widths at all ring longitudes. Figure 7 shows that, instead, there are significant variations in ring width that do not follow the simple width–longitude relation of Eq. (9).

For all of the rings, the rms residuals from the width–longitude fits are larger than the rms errors in the widths themselves. It appears that *none* of the nine rings is adequately modeled as having elliptical inner and outer edges in a fixed relative orientation: all of the rings have perturbed widths. The alternative is that the width errors have been underestimated, but we have taken care to include not only the formal error from the profile fit, but also the error due to uncertain stellar diameter, system time constant, and strip chart speed, where appropriate (see the Appendix). It is possible, of course, that the square-well model used to fit the profiles is inadequate, but this is unlikely to lead to erroneous width determinations if the rings are sharp-edged.

B. *Shepherd Satellite Width Perturbations*

Shepherd satellites could induce perturbations in ring widths, as well as in the local ring radius. Let W be the mean width of a circular ring perturbed by a shepherd satellite producing a sinusoidal perturbation of amplitude $\Delta r_{\max}$ in the ring. Then the width perturbation, ΔW, as a function of distance x along the ring's circumference is

$$\Delta W(x) = \Delta r_{\max}\left[\cos\left(\frac{2\pi x}{\lambda_o}\right) - \cos\left(\frac{2\pi x}{\lambda_i}\right)\right], \quad (10)$$

where λ_o and λ_i are the wavelengths of the perturbed outer and inner edges of the ring, respectively:

$$\lambda_o = 3\pi|a + W/2 - r|$$
$$\lambda_i = 3\pi|a - W/2 - r|. \quad (11)$$

At $x = 0$, the inner and outer edges are in phase, and $\Delta W \ll \Delta r_{\max}$. As the phase shift increases, $|\Delta W(x)|$ increases, and if $\Delta r_{\max} \geq W$, the wave breaks when adjacent particle trajectories intersect. If $\Delta r_{\max} \geq W$ and $|\lambda_o/\lambda_i - 1| \ll 1$, then the wave will break at a distance along the ring given approximately as

$$x_{\text{break}} \simeq \frac{3(a - r)^2}{2\Delta r_{\max}}. \quad (12)$$

If $x_{\text{break}} \gg \lambda = 3\pi|a - r|$, then the rms average of Eq. (10) over the region from $x = 0$ to $\lambda \ll x \ll x_{\text{break}}$ is

$$\Delta W_{\text{rms}} = \Delta r, \quad (13)$$

where, as before, Δr is the observed rms radius residual. In other words, in the zone where the wave has not broken, we expect mean width residuals to be comparable to radius residuals for shepherd-induced perturbations. After the wave breaks, both radius and width perturbations are damped out, until the next passage of the shepherd satellite near this region of the ring.

If we accept the width residuals as real, we have a curious situation. Typical rms width residuals, ΔW, range from 0.50 to 1.99 km (Table XIV), to be contrasted with orbit residuals, Δr, of less than 0.6 km for all but the γ and δ rings (Table XII). (The ratio of rms radius residual to rms width residual is included in Table XIV.) This suggests that width variations are roughly symmetrical about the mean orbit of each ring and are larger than the orbit residuals (except for γ and δ). This is quite different from the situation expected for perturbation from a shepherd satellite, where the width variations are *not* symmetric about the mean elliptical orbit, and are comparable to the deviations from the mean orbit [Eq. (13)].

The situation is somewhat different for

the γ and δ rings, for which $\Delta W < \Delta r$. The wide coverage of the 22 April 1982 occultation of KME14 enables us to "map" the widths and orbit residuals of these rings as a function of ring longitude, as shown in Figs. 3 and 4. The dashed lines sketch possible locations of the inner and outer ring edges for the unobserved regions of the rings. The solid lines represent plausible midlines of the rings. Of course, it is possible that there is considerable fine-scale structure as well, and in fact this is to be expected if shepherd satellites are present.

C. *Width–Radius Correlations*

As a further comparison of orbit perturbations and variations in ring width, we searched for correlations between ring orbit residuals, Δr, and residuals from width–longitude fits, ΔW. The results are shown in Fig. 8. For comparison, we formed the correlation plot corresponding to a ring perturbed by a shepherd several hundred kilometers away. Figure 9 (top) shows the inner and outer edges of the ring. They eventually get out of phase and collisional damping of the wave results. The corresponding correlation plot is shown in Fig. 9 (bottom).

The expectation that $\Delta W_{\max} \leq \Delta r_{\max}$ for shepherd-induced perturbations is violated for a number of rings, especially rings 4 and α, suggesting either that their width variations are not produced by shepherd satellites or that the observed perturbations are a complicated summation of effects from two or more shepherds.

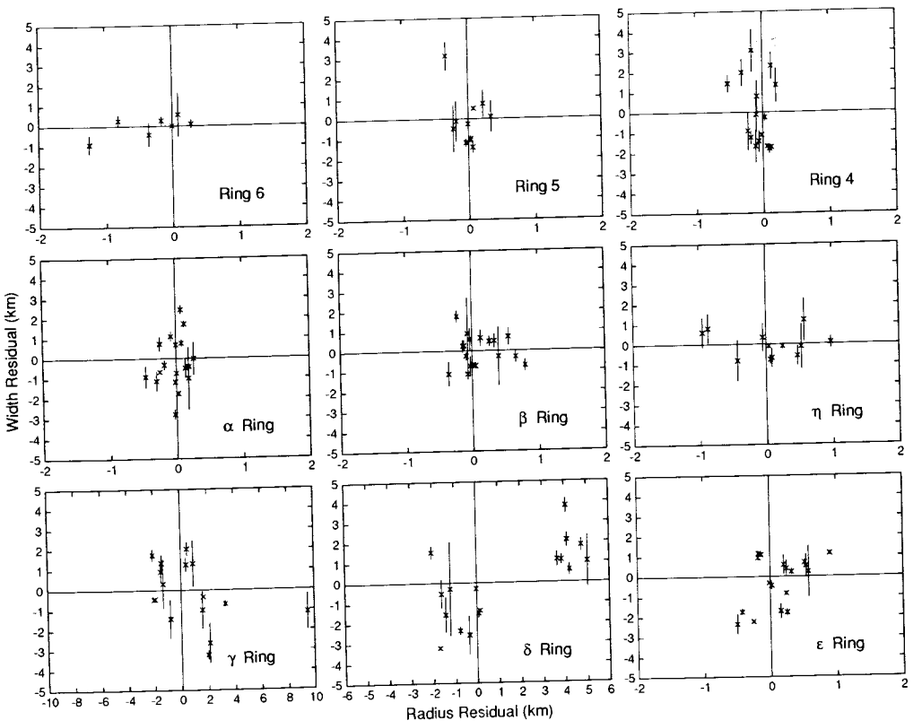

FIG. 8. Width residuals from width–longitude fits vs radius residuals from the ring orbit model. For several of the rings (4, α, and β, for example) width residuals are significantly larger than radius residuals. For the γ and δ rings, the opposite is true. If the rings are perturbed by shepherd satellites, width residuals would be comparable to radius residuals.

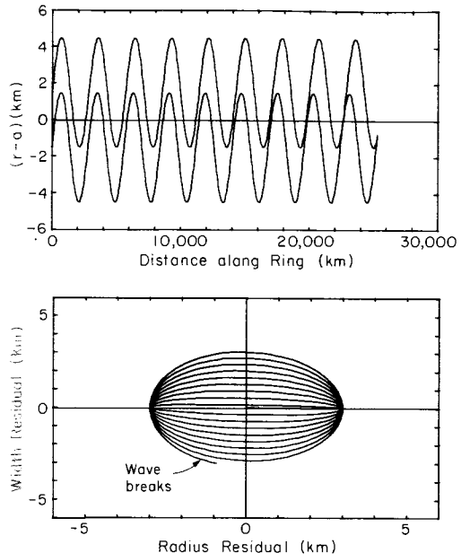

FIG. 9. Perturbations to a model ring due to a shepherd satellite several hundred kilometers from the ring. The upper figure shows the inner and outer edges of the ring as a function of distance along the ring. The sinusoidal variations gradually get out of phase, and in this simple model, the wave ultimately breaks. In a real ring, particle collisions would damp the wave before the ring pinched to this extent. The lower figure shows the residuals from the initial ring width vs the orbit radius residual of the midline of the model ring in the upper figure. At first, the radius residuals are larger than the width residuals. As the wave becomes out of phase, the width residuals increase to the point where they exceed the radius residuals. Ultimately, the wave breaks.

D. *Dynamical Properties of the Rings*

Using Borderies *et al.* (1983b) two-streamline model for a narrow eccentric ring, it is possible to determine ring masses, mean surface densities, velocity dispersions, and approximate ring thicknesses. We used their Eq. (28b) to solve for ring masses, and their Eqs. (33)–(34) [see Borderies *et al.* (1984) for a corrected version of Eq. (33b)] to solve for characteristic velocity dispersions for the α, β, and ε rings which have well-defined width–longitude relations. The results are tabulated in Table XV, which also includes mean surface densities for the rings, and Γ, the difference between the azimuth of maximum ring width and the azimuth of maximum distance from the planet. According to Borderies *et al.* (1983b), the two-streamline model may overestimate ring masses by about a factor of 2, compared to more accurate N-streamline calculations. Our results are roughly comparable to those of Nicholson and Matthews (1983), based on a smaller data set. We confirm that typical velocity dispersions are 0.2 cm sec^{-1}, giving a vertical scale height of the rings of about 8 m. As discussed by Cuzzi (1983), the rms velocities are governed by the size of largest particles. On this basis, we anticipate a cutoff on the upper size limit of particles on the order of 1 m.

V. RING OPACITIES

The opacity of a ring is directly related to a number of quantities of dynamical interest. If mass is proportional to optical depth, then the opacity profile gives the radial mass distribution. This determines the self-gravity of a ring, which may provide the torques necessary to prevent differential precession of an elliptical ring. As another example, the variation of mean opacity with ring width can be used to determine whether or not the ring particles form a monolayer.

In practice, our understanding of the optical depth profile of the Uranian rings is limited, not by the singnal-to-noise ratio of the data, but rather by Fresnel diffraction effects which limit the resolution to about 4 km at Uranus for the wavelengths of interest. Consequently, we have used a square-well model that represents a ring as a sharp-edged uniformly absoring translucent ("gray") screen. We begin by discussing the limitations of this approach, and then, mindful of these caveats, we investigate whether or not the rings are monolayers, and infer a number of dynamical properties of the rings.

TABLE XV

Kinematical and Dynamical Ring Parameters from Width-Longitude Fits			
Kinematical Ring Parameters	α	β	ε
a (km)	44726.6 ± 4.9	45668.8 ± 5.0	51156.3 ± 4.9
δa (km)	7.39 ± 0.31	8.79 ± 0.21	58.06 ± 0.26
e (x 10^3)	0.759 ± 0.026	0.438 ± 0.022	7.924 ± 0.023
δe (x 10^5)	5.8 ± 1.0	5.8 ± 0.8	75.8 ± 0.8
δω (deg)	-2.2 ± 0.7	-5.2 ± 0.9	(-0.01 ± 0.05)
Γ (deg) [a]	26 ± 8	35 ± 6	(0.1 ± 0.5)
a(δe/δa)	0.36 ± 0.06	0.30 ± 0.04	0.67 ± 0.01
ae(δω/δa)	-0.17 ± 0.05	-0.21 ± 0.03	(0.00 ± 0.01)
mean normal optical depth [b]	0.85 ± 0.04	0.46 ± 0.02	1.44 ± 0.05
Dynamical Ring Parameters [c]	α	β	ε
surface density (g cm^{-2}) [d]	2.0 ± 0.4	1.5 ± 0.2	32.7 ± 0.6
mass (g) [d]	(4.2 ± 0.9)x10^{16}	(3.8 ± 0.6)x10^{16}	(6.1 ± 0.1)x10^{18}
dispersion velocity (cm s^{-1})	0.15 ± 0.03	0.17 ± 0.02	(0.17 ± 0.43)

Notes:
(a) Γ is defined as the difference between the azimuth of maximum width and the azimuth of maximum distance from the planet.
(b) mean normal optical depth estimated as (mean equivalent depth)/δa, where no correction has been applied for diffraction effects.
(c) derived from the two-stream model of Borderies *et al.*, (1983b, 1984)
(d) N-streamline calculations indicate these might be too large by up to a factor of 2. All errors are formal errors.

A. *How Do We Define the Optical Depth of a Ring?*

It is evident that the gray-screen model is only a convenient approximation to the ring structure. There are clear and systematic variations in radial structure in the α, η, δ, and ε rings, and based on our knowledge of Saturn's rings, it is likely that all of the Uranian rings have radial structure that cannot be resolved from Earth-based observations. Furthermore, there are important diffraction effects that must be taken into account in order to relate the normal optical depth, as determined from square-well model fits, to physical properties of ring particles.

Accoding to the square-well model described in Paper I, the observed optical depth of a gray-screen ring τ_o is related to the observed fractional transmission, f_o, by

$$f_o = e^{-\tau_o}. \tag{14}$$

Then, under the assumption that the ring is many particles thick, the inferred optical depth normal to the ring τ_n is related to the observed value by

$$\tau_n = \tau_o \sin B, \tag{15}$$

where B is the viewing angle with respect to the ring plane.

Under *geometric optics*, the fractional area of the ring surface not shadowed by particles would be given by $e^{-\tau_n}$. However, the actual situation is considerably more complicated because diffraction effects are extremely important. P. Nicholson (private communication) has investigated Fresnel diffraction by "zebra-striped" ($\tau = 0$ or ∞ for alternate strips) and uniform gray screens, and has shown that, "for a zebra ring with a fractional area of clear space = f_z, the near on-axis diffraction pattern is equivalent to that produced by a grey ring of the same overall width, but with an intensity transmission of $f_G = f_z^2$. Expressing both transmission factors in terms of optical depth . . . we have $\tau_G = 2\tau_z$." This is consistent with Cuzzi's (1985) conclusion that the gray screen optical depth obtained from stellar occultations is twice the fractional area physically filled by particles, which is used to infer both particle reflectivity and particle size, although Nicholson points out that the multiplicative factor may be smaller than 2 for rings that contain strips (of higher or lower optical depth than the average) that have widths comparable to a Fresnel zone. The ε ring may be an example of this. We emphasize *that our reported normal optical depths, τ_n, must be corrected for diffraction effects before being used to infer ring particle properties.*

As an additional caution we note that, quite independent of diffraction effects, the gray-screen normal optical depth is computed as

$$\tau_n = -\sin B \ln \int_{-W/2}^{W/2} \frac{f_o(r)dr}{W}, \tag{16}$$

whereas the radially averaged normal optical depth is actually

$$\langle \tau_n \rangle = -\sin B \int_{-W/2}^{W/2} \frac{\ln f_o(r)dr}{W}. \tag{17}$$

In these equations, $f_o(r)$ is observed fractional transmission as a function of ring radius, after effects of stellar image size, instrumental response, and diffraction have been removed. The logarithmic weighting of the integrand in Eq. (17) has the effect that $\tau_n < \langle \tau_n \rangle$ for rings that have significant variations in radial structure.

To summarize:

(1) In this paper and in Paper I, the normal optical depth, τ_n, is computed by assuming that the ring is a gray screen, many particles thick.

(2) The gray-screen optical depth, τ_n, must be corrected for diffraction effects (i.e., reduced by roughly a factor of 2, depending on the details of the particle size distribution) before being used to infer ring particle properties. (The factor of 2 is likely to be valid for almost all particle sizes up to 100 m or so.)

(3) Independent of (2), τ_n is not a rigorous mean optical depth of a ring because it is obtained by radially averaging the fractional transmission across the ring, rather than radially averaging the normal optical depth.

Of course, a complete model relating the "observed" gray-screen optical depth, τ_o, to the properties of a ring must take into account the viewing geometry, the wavelength of the observations, and the radial and vertical distribution of ring particles, as well as their scattering functions.

B. *Are the Rings Monolayers?*

Saturn's rings are known to be extremely thin—perhaps as little as 10 m—(Lane *et al.*, 1982; Marouf and Tyler, 1982; Porco *et al.*, 1984b; Zebker and Tyler, 1984), and dynamical arguments (Cuzzi *et al.*, 1979a, 1979b) imply that a characteristic thickness of a ring is a few times the diameter of the largest particles: dynamically, rings can be regarded as monolayers. For a true monolayer, there is no shadowing by neighboring particles until the ring is observed nearly edge-on. In the absence of such shadowing, the "equivalent width," E [defined as the product of the fraction of the light scattered and/or absorbed by the ring and the projected width of the ring; see Eq. (5) of Paper I], of a ring is independent of ring width, as long as the linear mass density of the ring is constant and the particle size distribution is independent of ring longitude. The ring would then be both a dynamical and an optical monolayer.

On the other hand, since the area-to-mass ratio increases for smaller particles, it is possible for most of the mass to reside in large particles which form an effective monolayer, and most of the area to reside in a many-particles-thick layer of smaller particles (Wiedenschilling *et al.*, 1984). Under these circumstances, the observed opacity of the ring is controlled by the distribution of small particles, and the radially integrated optical depth, rather than the equivalent width, is expected to be invariant for a ring. In the context of the square-well model, the "equivalent depth," A [defined as the product of the ring width and the normal optical depth; see Eq. (6) of Paper I], of a ring would then be conserved, to the extent that the optical depth is uniform across the ring.

The intermediate case has been explored by Zebker *et al.* (1985), who have developed a scattering model that allows the vertical ring profile to vary from a near monolayer to a many-particles-thick system. The model has been used to study Voyager ob-

servations of microwave scatter from planetary rings, but is not directly applicable to stellar ring-occultation observations because both the intensity and the phase of the diffracted radiation must be recorded.

We have determined the equivalent widths and equivalent depths for all ring profiles, in order to test whether or not the rings behave as optical monolayers. Several fits were performed. First, we determined the mean equivalent width and depth for each ring. If the equivalent depth is constant for all ring profiles, then the equivalent width can be expressed as a function of ring width:

$$E(W) = \frac{\bar{A}}{\tau_o(W)}\left(1 - e^{-\tau_o(W)}\right), \qquad (18)$$

where τ_o is the optical depth of the model profile. We then fitted the equivalent width data, using Eq. (18), for the mean equivalent depth, $\bar{A}$. Finally, for the rings with well-established width–longitude relations (α, β, and ε), we used the width as defined by the width–longitude relation, rather than

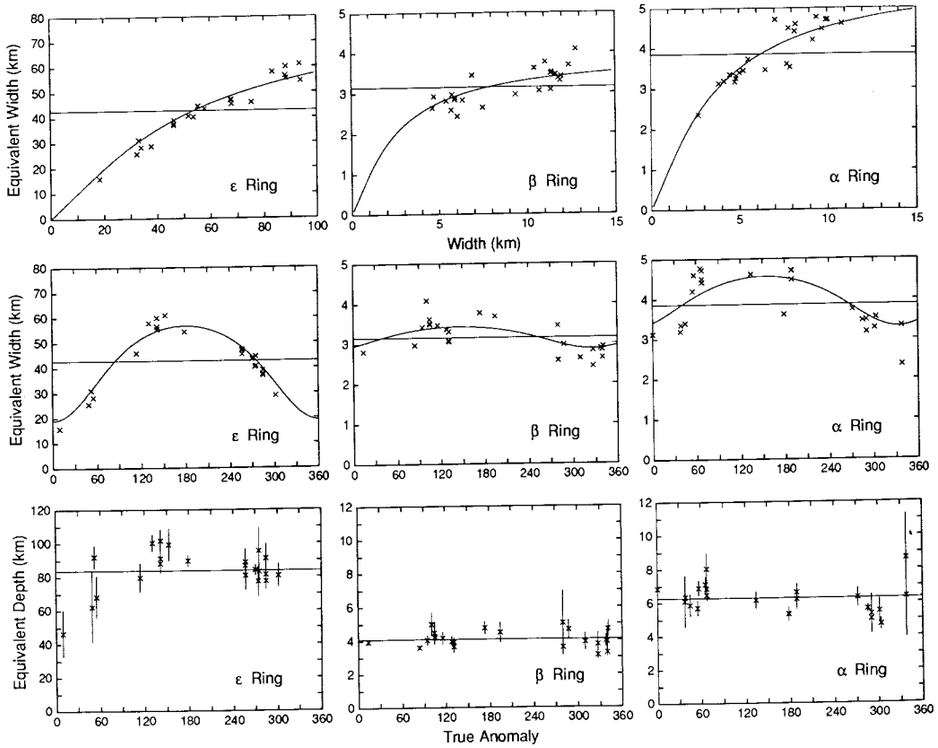

FIG. 10. Equivalent widths and equivalent depths of the ε, β, and α rings. The top row of figures shows the equivalent width, E, as a function of ring width. The horizontal line is the mean equivalent width as given in Table XVI, fitted to all ring profiles for which the equivalent width (but not necessarily the ring width) were accurately determined. The curve line is the best-fitting constant equivalent depth model, for all ring profiles for which both equivalent width and equivalent depth were accurately determined. The middle row of figures plots the equivalent widths as a function of true anomaly. The horizontal line is the mean equivalent width, as above, and the curved line is the best-fitting constant equivalent depth model, using the width–longitude relation for each ring to relate ring width and true anomaly. The botton row of figures shows the equivalent depth, A, as a function of true anomaly, and the best-fitting mean value.

the measured width, and used Eq. (18) to determine the mean equivalent depth.

Figure 10 shows the results for the α, β, and ε rings. The top two rows show the equivalent width as a function of measured ring width and true anomaly, respectively. In each figure, the horizontal line is the best-fitting mean equivalent width. The curved line is the best fit to the data under the assumption that the equivalent *depth* is conserved, instead. The bottom row of figures shows the equivalent depth as a function of true anomaly, with the best-fitting mean value shown as a horizontal line.

The results for the other rings are shown in Figs. 11 and 12. Table XVI contains the numerical results of each of the fits. For every ring, the equivalent depth fit using Eq. (18) is a better fit to the equivalent width data than the optical monolayer model of a constant equivalent width. On the other hand, Figs. 10–12 show that, for most rings, there are significant deviations from constant equivalent depth. We draw the following conclusions from these results:

(1) The rings are not optical monolayers. For the rings with significant optical depth, their equivalent width clearly increases with ring width, an indication that particles shadow each other. For the optically thin rings, the effect is not as marked, but the rms residuals of the fits to the equivalent width data are in every case lower when Eq. (18) is used than when the equivalent width is modeled as constant.

(2) The equivalent depths of some rings have significant variations from the average value. This can be due either to longitudinal clumping of ring material (i.e., the linear mass density varies with ring longitude), or to nonuniform radial mass distribution (in which case the equivalent depth obtained from the square-well model is not a valid measure of the quantity, $\int \tau_n(r)dr$). Because Saturn's narrow ringlets have considerable

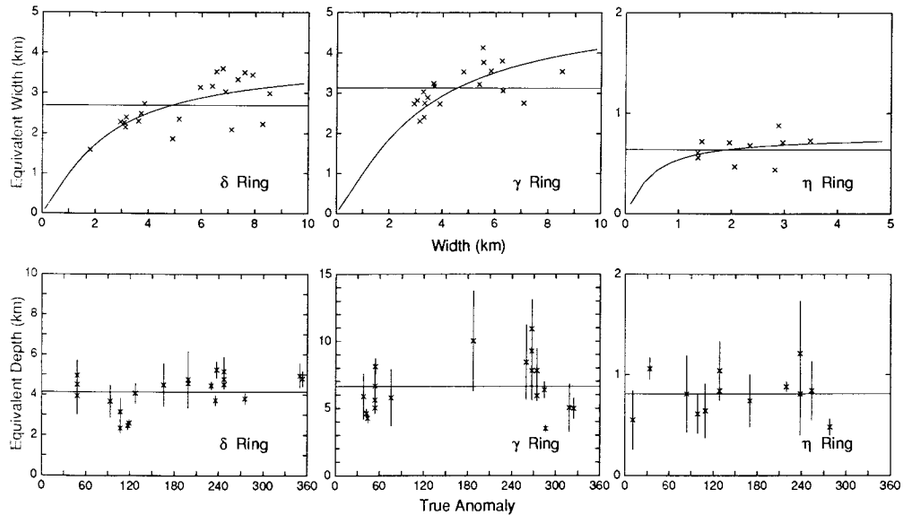

FIG. 11. Equivalent widths and equivalent depths of the δ, γ, and ε rings. The top row of figures shows the equivalent width, E, as a function of ring width. The horizontal line is the mean equivalent width as given in Table XVI, fitted to all ring profiles for which the equivalent width (but not necessarily the ring width) were accurately determined. The curved line is the best-fitting constant equivalent depth model, for all ring profiles for which both equivalent width and equivalent depth were accurately determined. The botton row of figures shows the equivalent depth, A, as a function of true anomaly, and the best-fitting mean value.

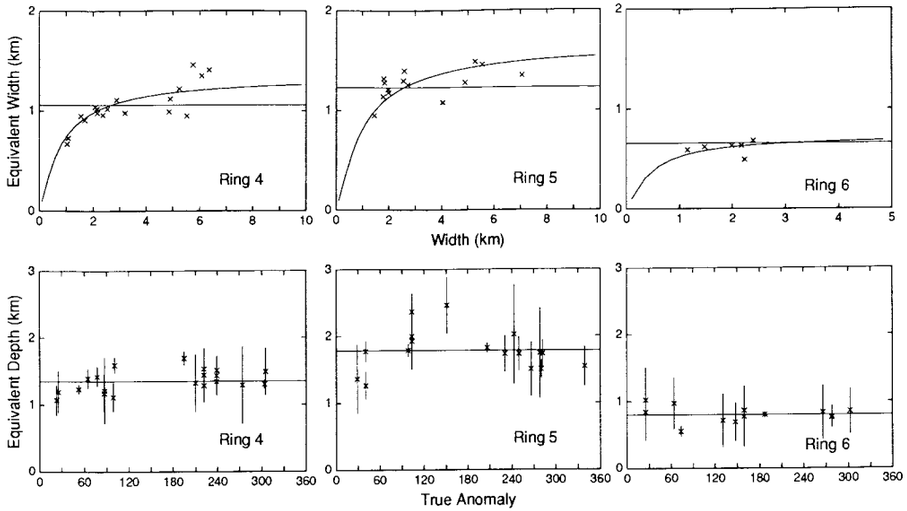

FIG. 12. Equivalent widths and equivalent depths of the 4, 5, and 6. The top row of figures shows the equivalent width, E, as a function of ring width. The horizontal line is the mean equivalent width as given in Table XVI, fitted to all ring profiles for which the equivalent width (but not necessarily the ring width) were accurately determined. The curved line is the best-fitting constant equivalent depth model, for all ring profiles for which both equivalent width and equivalent depth were accurately determined. The botton row of figures shows the equivalent depth, A, as a function of true anomaly, and the best-fitting mean value.

fine-scale radial structure, we prefer the latter explanation, and regard these results as independent evidence that there is significant unresolved structure in the rings.

(3) If rings are dynamical monolayers, but not optical monolayers, then the particle size distribution must be such that the small particles govern the opacity of the rings. Let us assume a power law distribution of particle sizes of the form

$$n(a) = n(a_0)\left(\frac{a}{a_0}\right)^{-q} \qquad (19)$$

[Eq. (17), Paper I], where $n(a)da$ is the column density of particles with radii between a and $a + da$, a_0 is an arbitrary reference radius, and q is the power law index. The condition that small particles are responsible for most of the shadowing constrains q to be greater than 3. Since q is close to 3 for Saturn's rings (Marouf *et al.*, 1983), the power law indices for the two ring systems may be quite similar.

VI. DISCUSSION AND CONCLUSIONS

Using Uranus ring occultation observations obtained from 1977 to 1983, we have been able to refine the kinematical model for the nine known rings. The improvements over earlier models are due primarily to the exclusion of strip chart data, the use of a square-well model to determine mid-times for all of the rings, and the recognition that the γ and δ rings deviate significantly from Keplerian ellipses. It is now clear that high time resolution, accurate absolute timing, and long north–south baselines are essential to further refinement of the orbital elements. With the inclusion of additional multiple-site observations, J_4 can be determined with sufficient accuracy to be a useful constraint on interior models of Uranus. There is still some uncertainty in the pole direction, because of an apparent incompatibility between two data sets. This problem should also be resolved by further observations.

Typical post-fit residuals of 0.2–0.6 km in ring plane radius for all but the γ and δ rings place stringent limits on sizes of possible shepherd satellites, as shown in Fig. 2. For example, we find an upper limit of about 17 km for the diameter of a shepherd satellite of density 1.5 g cm^{-3} located 100 km from the ε ring. Rms residuals of 3 km for the γ and δ rings may be due to nearby shepherds, although there is also the possibility that Lindblad resonances associated with the rings produce the observed perturbations.

From the ring width determinations, it is certain that all nine rings have significant width perturbations. The narrow eccentric rings 6, 5, and 4 do not have linear width–longitude relations, there is significant scatter in the width–longitude relations for rings α, β, and ε, and the narrow quasi-circular rings γ, δ, and η all have large width variations. Shepherd satellites may be responsible for these perturbations, but the simplest model that can account for the magnitude of the observed width variations predicts radial perturbations somewhat larger than what are observed.

It is now clear that the Uranian rings are not optical monolayers—there is significant particle shadowing for all nine rings. The inferred normal optical depths must be corrected for diffraction effects before they are used to constrain the physical properties of the ring material. The "equivalent depths" of the γ and δ rings are not conserved, probably indicative of unresolved radial structure within the rings.

We are still left with a number of puzzles:

- Why do the narrow rings not follow width–longitude relations? If shepherd satellites are responsible, why are the width perturbations typically much larger than the radial perturbations?
- What perturbs the γ and δ rings? Are internal instabilities, shepherd satellites, or more distant satellites with nearby Lindblad resonances responsible?
- Why is the "equivalent depth" of the γ and δ rings so variable? Is it due to longitudinal clumping, or to complex radial structure that varies with ring longitude?

Continued Earth-based surveillance of the Uranian rings and the recent Voyager encounter will help to answer some of these questions. There are certain to be significant improvements in the orbital elements, pole direction, and J_2 and J_4. Comparison with Saturn's rings should also yield important clues about the structure and dynamics of Uranus' ring system.

TABLE XVI

Results of Equivalent Width and Depth Fits

Ring	Fits to Equivalent Width Data		Fits to Equivalent Depth Data			
	Mean Equivalent Width (km)	rms residual (km)	Mean Equivalent Depth (km)	rms residual (km)	Mean Equivalent Depth (km)	rms residual (km)
6	0.66 ± 0.03	0.12	0.74 ± 0.04	0.06	0.80 ± 0.03	0.12
5	1.23 ± 0.04	0.17	1.68 ± 0.07	0.14	1.78 ± 0.08	0.32
4	1.06 ± 0.05	0.20	1.35 ± 0.05	0.12	1.35 ± 0.04	0.16
α	3.86 ± 0.15	0.70	6.02 ± 0.15	0.30	6.29 ± 0.19	0.91
β	3.16 ± 0.09	0.43	4.02 ± 0.09	0.28	4.08 ± 0.10	0.51
η	0.64 ± 0.03	0.12	0.78 ± 0.06	0.13	0.81 ± 0.05	0.20
γ	3.13 ± 0.11	0.49	5.29 ± 0.29	0.42	6.63 ± 0.47	2.04
δ	2.69 ± 0.13	0.61	3.93 ± 0.20	0.44	4.14 ± 0.19	0.87
ε	42.76 ± 2.57	12.03	85.15 ± 2.50	3.08	83.83 ± 2.73	12.79

APPENDIX

ERROR ESTIMATE FOR RING WIDTHS AND EQUIVALENT DEPTHS

The least-squares fitting procedure described in Paper I yields formal errors for all fitted parameters, but the true uncertainties may be much larger, due to uncertainties in quantities that were held fixed during the fit. In particular, imperfect knowledge of n_*, the unocculted star level, T_*, the stellar diameter, and t_c, the instrumental time constant, contributes importantly to the overall uncertainty. Additionally, in those cases where ring profiles were digitized from strip chart records, uneven chart

speed introduces some error. We describe here the procedures we used to estimate more realistic errors for ring widths and equivalent depths, by taking these factors into account.

A. *Errors in Ring Width*

The width of a ring is given by $W = v_r T_o$, where v_r is the apparent radial velocity of the star in the ring plane and T_o is the duration of the occultation profile of the model ring (see Paper I). Since v_r is determined accurately from event astrometry, errors in W are proportional to errors in T_o.

(*1*) *Uncertain stellar diameter, T_*.* Ring profiles are significantly distorted when the projected width of the ring is smaller than the projected size of the occulted star. In these cases, there is a strong correlation between the adopted stellar diameter and the ring width determined from the fit. Since stellar diameters are uncertain (Table II), it is important to estimate the corresponding uncertainty this introduces into the ring widths. We performed a number of fits to a variety of ring profiles, varying the adopted stellar diameter to determine the corresponding change in the fitted ring width. The results are shown in Fig. A-1, where we have plotted the fractional change in the fitted width ($\delta T_o/T_o$) divided by the fractional change in the stellar diameter ($\delta T_*/T_*$), against the ring width in units of the stellar diameter (T_o/T_*). There is a clear trend in the distribution of points, approximated by the smooth curve in the figure. Notice that, for narrow rings, a small change in the adopted stellar diameter introduces a relatively large change in the resulting ring width.

Based on these results, we approximate the error in the duration, T_o, introduced by uncertainty in the star size as

$$\sigma_{T_*}(T_o) = \frac{\delta T_o}{\delta T_*}\,\sigma(T_*). \qquad \text{(A-1)}$$

All of the quantities on the right hand side are known from the fit, from Table II, and from the calibration curve in Fig. A-1.

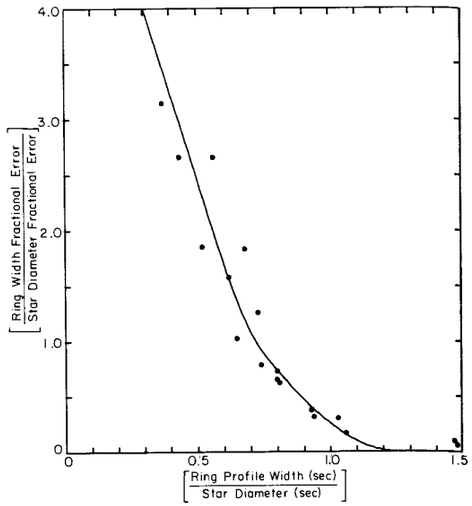

FIG. A-1. The uncertainty in the ring width derived from a profile fit, due to an uncertainty in the projected stellar diameter. The dots represent results from fits to occultation data wherein the stellar diameter was changed and the corresponding change in derived ring width was determined. The smooth curve is the calibration used for the data presented in this paper.

(*2*) *Uncertain time constant, t_c.* We used a similar approach to determine the effects of an uncertain time constant. Figure A-2 shows the fractional change in the fitted width, divided by the fractional change in the adopted time constant ($\delta t_c/t_c$), plotted against the ring width in units of the time constant, T_o/T_c. Again, the points are well approximated by the smooth curve. We approximate the error in the duration, T_o, introduced by uncertainty in the time constant as

$$\sigma_{t_c}(T_o) = \frac{\delta T_o}{\delta t_c}\,\sigma(t_c), \qquad \text{(A-2)}$$

where $\sigma(t_c)$ is the estimated uncertainty in the system time constant.

(*3*) *Uneven chart speed.* We estimate the unevenness of the speed of a chart recorder by measuring the separation of adjacent one-second tick marks on the chart record. The standard deviation of the distribution of such points is comparable to the uncertainty in measuring the duration of a typical

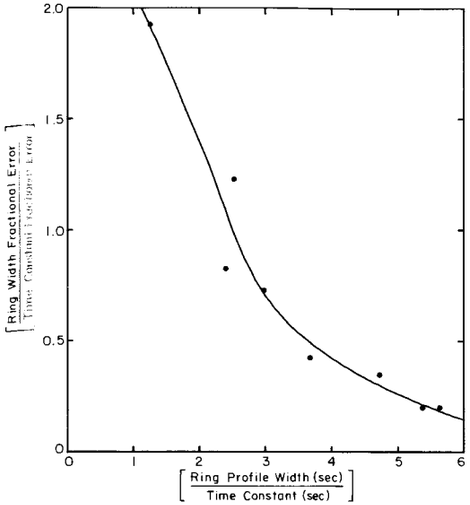

FIG. A-2. The uncertainty in the ring width derived from a profile fit, due to an uncertainty in the instrumental time constant. The dots represent results from fits to occultation data wherein the time constant was changed and the corresponding change in derived ring width was determined. The smooth curve is the calibration used for the data presented in this paper.

ring profile due to uneven chart speed. We define this uncertainty as $\sigma_{\text{chart}}(T_o)$.

(*4*) *Uncertain star level, $\bar{n}_*$.* Test results have shown that fitted ring widths are not strongly correlated with $\bar{n}_*$, and we have therefore made no correction to the width error due to uncertain $\bar{n}_*$.

(*5*) *Final estimate of width error.* Under the assumption that all sources of error are uncorrelated, we define the effective uncertainty in the ring width as

$$\sigma_{\text{eff}}(W) = [\sigma^2_{\text{fit}}(W) + \sigma^2_{\text{other}}(W)]^{1/2}, \qquad \text{(A-3)}$$

where

$$\sigma_{\text{other}}(W) = v_r[\sigma^2_{T_*}(T_o) + \sigma^2_{t_c}(T_o) + \sigma^2_{\text{chart}}(T_o)]^{1/2}. \qquad \text{(A-4)}$$

B. *Errors in Equivalent Depth*

The equivalent depth of a ring is defined (see Paper I) as

$$A = W\tau_o \sin B, \qquad \text{(A-5)}$$

where τ_o is the observed gray-screen optical depth of the ring and B is the viewing angle, measured with respect to the plane of the ring. The gray-screen optical depth is related to the fractional transmission of the ring, f_o, by

$$f_o = e^{-\tau_o}. \qquad \text{(A-6)}$$

We can rewrite the equivalent depth as

$$A = -W \ln(f_o)\sin B \qquad \text{(A-7)}$$

and approximate the effective error in A as

$$\sigma_{\text{eff}}(A) = [\sigma^2_{\text{fit}}(A) + \sigma^2_{\text{other}}(A)]^{1/2}, \qquad \text{(A-8)}$$

where $\sigma_{\text{fit}}(A)$ is the formal error in A, given by the model fit, and $\sigma^2_{\text{other}}(A)$ is the variance in A due to uncertainties in T_*, t_c, chart speed, and $\bar{n}_*$. The first three of these contribute primarily to an uncertainty in W, whereas $\bar{n}_*$ enters directly into the determination of f_o. Therefore, we approximate $\sigma^2_{\text{other}}(A)$ as

$$\sigma^2_{\text{other}}(A) \approx \left(\frac{A}{W}\right)^2 \sigma^2_{\text{other}}(W) + \left(\frac{A}{f_o \ln f_o}\right)^2 \sigma^2(f_o), \qquad \text{(A-9)}$$

where we assume

$$\sigma(f_o) = (1 - f_o)\sigma(\bar{n}_*)/\bar{n}_*, \qquad \text{(A-10)}$$

the fractional uncertainty in the mean unocculted star count rate.

ACKNOWLEDGMENTS

We thank André Brahic, Ian Glass, Keith Matthews, Philip Nicholson, and Bruno Sicardy for access to their observations prior to publication. Philip Nicholson and Richard Greenberg refereed the original manuscript with admirable thoroughness. Karen Lasky and Karen Meech helped with the data analysis. We thank Scott Tremaine for several productive discussions. S.E.L. gratefully acknowledges the assistance of the Undergraduate Research Opportunities Program at MIT. This work was supported in part by NASA Grants NAGW-656 and NSG-7526, and by NSF Grant AST-829825.

REFERENCES

BHATTACHARYYA, J. C., AND M. K. V. BAPPU (1977). Saturn-like ring system around Uranus. *Nature* **270,** 503–506.

BORDERIES, N., P. GOLDREICH, AND S. TREMAINE (1983a). The variations in eccentricity and apse precession rate of a narrow ring perturbed by a close satellite. *Icarus* **53,** 84–89.

BORDERIES, N., P. GOLDREICH, AND S. TREMAINE (1983b). The dynamics of elliptical rings. *Astron. J.* **88,** 1560–1568.

BORDERIES, N., P. GOLDREICH, AND S. TREMAINE (1984). Erratum: "The dynamics of elliptical rings." *Astron. J.* **89,** 727.

BORDERIES, N., P. GOLDREICH, AND S. TREMAINE (1985). A granular flow model for dense planetary rings. *Icarus* **63,** 406–420.

CHEN, D.-H., H.-Y. YANG, C.-H. WU, Y.-C. WU, S.-Y. KIANGA, Y.-W. HUANG, C.-T. YEH, T.-S. CHAI, C.-C. HSIEH, C.-S. CHENG, AND C. CHANG (1978). Photoelectric observation of the occultation of SAO 158687 by Uranian ring and detection of Uranian ring signals from the light curve. *Scientia Sinica* **XXI,** 503–508.

CUZZI, J. (1983). Planetary ring systems. *Rev. Geophys. Space Phys.* **21,** 173–186.

CUZZI, J. N. (1985). Rings of Uranus: Not so thick, not so black. *Icarus* **63,** 312–316.

CUZZI, J. N., R. H. DURISEN, J. A. BURNS, AND P. HAMMILL (1979a). The vertical structure and thickness of Saturn's rings. *Icarus* **38,** 54–68.

CUZZI, J. N., J. A. BURNS, R. H. DURISEN, AND P. M. HAMMILL (1979b). The vertical structure and thickness of Saturn's rings. *Nature* **281,** 202–204.

CUZZI, J. N., AND J. D. SCARGLE (1985). Wavy edges suggest moonlet in Encke's gap. *Astrophys. J.* **292,** 276–290.

DERMOTT, S., AND P. NICHOLSON (1986). The masses of the Uranian satellites. *Nature* **319,** 115–120.

ELLIOT, J. L., E. DUNHAM, L. H. WASSERMAN, R. L. MILLIS, AND J. CHURMS (1978). The radii of Uranian rings α, β, γ, δ, ε, η, 4, 5, and 6 from their occultation of SAO 158687. *Astron. J.* **83,** 980–992.

ELLIOT, J. L., J. H. ELIAS, R. G. FRENCH, JAY FROGEL, W. LILLER, K. MATTHEWS, K. J. MEECH, D. J. MINK, P. D. NICHOLSON, AND B. SICARDY (1983). The rings of Uranus: Occultation profiles from three observatories. *Icarus* **56,** 202–208.

ELLIOT, J. L., R. G. FRENCH, J. A., FROGEL, J. H. ELIAS, D. M. MINK, AND W. LILLER (1981a). Orbits of nine Uranian rings. *Astron. J.* **86,** 444–455.

ELLIOT, J. L., J. A. FROGEL, J. H. ELIAS, I. S. GLASS, R. G. FRENCH, D. J. MINK, AND W. LILLER (1981b). The 20 March 1980 occultation by the Uranian rings. *Astron. J.* **86,** 127–134.

ELLIOT, J. L., R. G. FRENCH, K. J. MEECH, AND J. H. ELIAS (1984). Structure of the Uranian rings. I. Square-well model and particle-size constraints. *Astron. J.* **89,** 1587–1603.

ELLIOT, J. L., AND P. D. NICHOLSON (1984). The rings of Uranus. In *Planetary Rings* (A. Brahic and R. Greenberg, Eds.), pp. 25–72. Univ. of Arizona Press, Tucson.

ESHLEMAN, V. R., J. V. BREAKWELL, G. L. TYLER, AND E. A. MAROUF (1983). W-shaped occultation signatures: Inference of entwined particle orbits in charged planetary ringlets. *Icarus* **54,** 212–226.

FREEDMAN, A., S. D. TREMAINE, AND J. L. ELLIOT (1983). Weak dynamical forcing of the Uranian ring system. *Astron. J.* **88,** 1053–1059.

FRENCH, R. G., R. L. BARON, J. L. ELLIOT, L. M. FRENCH, J. A. KANGAS, K. J. MEECH, M. RESSLER, J. FROGEL, J. JIMENEZ, M. JOY, E. F. ERICKSON, K. MATTHEWS, B. T. SOIFER, G. NEUGEBAUER, AND P. NICHOLSON (1985). The 4 May and 24 May 1985 Occultations by the Uranian rings. *Bull. Amer. Astron. Soc.* **17,** 718.

FRENCH, R. G., J. L. ELLIOT, AND D. A. ALLEN (1982). Inclinations of the Uranian rings. *Nature* **298,** 827–829.

FRENCH, R. G., T. J. JONES, AND A. R. HYLAND (1986a). The 1 May 1982 stellar occultation by Uranus and the rings: Observations from Mount Stromlo Observatory. In press.

FRENCH, R. G., J. A. KANGAS, AND J. L. ELLIOT (1986b). What perturbs the γ and δ rings of Uranus? *Science* **231,** 480–483.

GOLDREICH, P., AND S. TREMAINE (1979a). Towards a theory for the Uranian rings. *Nature* **277,** 97–99.

GOLDREICH, P., AND S. TREMAINE (1979b). Precession of the ε ring of Uranus. *Astron. J.* **84,** 1678–1691.

HUBBARD, W. B., AND B. H. ZELLNER (1980). Results from the 10 March 1977 occultation by the Uranian system. *Astron. J.* **85,** 1663–1669.

IAUC (1983). *Occultations by Uranus II (Umbriel) on 1983 March 25.* IAU Circ. No. 3784.

JABLONSKI, F. J., AND J. BARROSO, JR. (1985). The April 22 occultation of Hyd-20°51699 by Uranus and its rings. *Astron. Astrophys.* **144,** 249–250.

KLEMOLA, A. R., AND B. G. MARSDEN (1977). Predicted occultations by the rings of Uranus, 1977–1980. *Astron. J.* **82,** 849–851.

KLEMOLA, A. R., D. J. MINK, AND J. L. ELLIOT (1981). Predicted occultations by Uranus: 1981–1984. *Astron. J.* **86,** 138–140.

LANE, A. L., R. B. POMPHREY, R. B. MORRIS, C. W. HORD, R. A. WEST, L. W. ESPOSITO, F. E. SIMMONS, D. L. COFFEEN, AND M. SATO (1982). Photopolarimetry from Voyager 2—preliminary results on Saturn, Titan, and the rings. *Science* **215,** 537–543.

MAHRA, H. S., AND S. K. GUPTA (1977). *Occultation of SAO 158687 by the Uranian Rings.* IAU Circ. No. 3061.

MAHRA, H. S., A. K. PANDEY, U. C. JOSHI, AND V. MOHAN (1983). The occultation of BD-19 4222 by Uranus on 1981 April 26. *Bull. Astron. Soc. India II,* 152–158.

MAROUF, E. A., AND G. L. TYLER (1982). Microwave edge diffraction by features in Saturn's rings—observations with Voyager 1. *Science* **217,** 243–245.

MAROUF, E. A., G. L. TYLER, H. A. ZEBKER, R. A. SIMPSON, AND V. R. ESHLEMAN (1983). Particle-size distributions in Saturn's rings from Voyager 1 radio occultation. *Icarus* **54,** 189–211.

MILLIS, R. L., L. H. WASSERMAN, AND R. G. FRENCH (1986). Observations of the 22 April 1982 stellar occultation by Uranus and the rings. In press.

MILLIS, R. L., AND L. H. WASSERMAN (1978). The occultation of BD-15° 3969 by the rings of Uranus. *Astron. J.* **83,** 993–998.

MILLIS, R. L., L. H. WASSERMAN, AND P. BIRCH (1977a). Detection of rings around Uranus. *Nature* **267,** 330–331.

MILLIS, R. L., L. H. WASSERMAN, J. L. ELLIOT, AND E. W. DUNHAM (1977b). The rings of Uranus: Their widths and optical thicknesses. *Bull. Amer. Astron. Soc.* **9,** 498.

MINER, E. D., A. INGERSOLL, L. ESPOSITO, T. JOHNSON, AND R. WESSEN (1985). *Science Objectives and Preliminary Sequence Designs for the Voyager, Uranus and Neptune Encounters.* Report of the Uranus/Neptune Science Working Groups. NASA Publication 1618-57, pp. 32–34.

NICHOLSON, P. D., AND K. MATTHEWS (1983). Surface densities and velocity dispersons of the Uranian rings. *Bull. Amer. Astron. Soc.* **15,** 816.

NICHOLSON, P. D., K. MATTHEWS, AND P. GOLDREICH (1981). The Uranus occultation of 10 June 1979. I. The rings. *Astron. J.* **87,** 433–447.

NICHOLSON, P. D., K. MATTHEWS, AND P. GOLDREICH (1982). Radial widths, optical depths, and eccentricities of the Uranian rings. *Astron. J.* **87,** 433–447.

NICHOLSON, P. D., S. E. PERSSON, K. MATTHEWS, P. GOLDREICH, AND G. NEUGEBAUER (1978). The rings of Uranus: Results of the 10 April 1978 occultation. *Astron. J.* **83,** 1240–1248.

PORCO, C., G. E. DANIELSON, P. GOLDREICH, J. B. HOLBERG, AND A. L. LANE (1984a). Saturn's axisymmetric ring edges at $1.95R_s$ and $2.27R_s$. *Icarus* **60,** 17–28.

PORCO, C., P. D. NICHOLSON, N. BORDERIES, G. E. DANIELSON, P. GOLDREICH, J. B. HOLBERG, AND A. L. LANE (1984b). The eccentric Saturnian ringlets at $1.29R_s$ and $1.45R_s$. *Icarus* **60,** 1–16.

SICARDY, B., P. BOUCHET, C. PERRIER, A. BRAHIC, J. LECACHEUX, AND P. LAQUES (1985). *Les occultations du 15 Aout 1980 et du 22 Avril 1982 par les anneaux d'Uranus.* Preprint.

SICARDY, B., A. BRAHIC, J. LECACHEUX, P. BOUCHET, C. PERRIER, P. LAQUES, AND J. LEGAIT (1982a). The occultation of the star KME14 by Uranus rings (22 April 1982). *Bull. Amer. Astron. Soc.* **14,** 749.

SICARDY, B., M. COMBES, A. BRAHIC, P. BOUCHET, C. PERRIER, AND R. COURTIN (1982b). The 15 August 1980 occultation by the Uranian system: Structure of the rings and temperature of the upper atmosphere. *Icarus* **52,** 459–472.

SICARDY, B., M. COMBES, J. LECACHEUX, P. BOUCHET, A. BRAHIC, P. LAQUES, C. PERRIER, L. VAPILLON, AND Y. ZEAU (1985). Variations of the stratospheric temperature along the limb of Uranus: Results of the 22 April 1982 stellar occultation. *Icarus* **64,** 99–106.

STANDISH, E. M. (1982). Orientation of JPL Ephemerides DE-200/LE-200 to the dynamical equinox of J2000. *Astron. Astrophys.* **114,** 297–302.

VEILLET, C. (1983). *De l'observation et du mouvement des satellites d'Uranus.* Thesè de Doctorat d'Etat, Université de Paris 6.

WIEDENSCHILLING, S. J., C. R. CHAPMAN, D. R. DAVIS, AND R. GREENBERG (1984). Ring particles: Collisional interactions and physical nature. In *Planetary Rings* (A. Brahic and R. Greenberg, Eds.), pp. 367–415. Univ. of Arizona Press, Tucson.

ZEBKER, H. A., E. A. MAROUF, AND G. L. TYLER (1985). Saturn's rings: Particle size distributions for thin layer models. *Icarus* **64,** 531–548.

ZEBKER, H. A., AND G. L. TYLER (1984). Thickness of Saturn's rings inferred from Voyager 1 observations of microwave scatter. *Science* **223,** 396–398.